REVIEW

Check for updates

Unsupervised learning and pattern recognition in alloy design

Ninad Bhat,[a] Nick Birbilis[b] and Amanda S. Barnard [ID] *[c]

Machine learning has the potential to revolutionise alloy design by uncovering useful patterns in complex datasets and supplementing human expertise and experience. This review examines the role of unsupervised learning methods, including clustering, dimensionality reduction, and manifold learning, in the context of alloy design. While the use of unsupervised learning in alloy design is still in its early stages, these techniques offer new ways to analyse high-dimensional alloy data, uncovering structures and relationships that are difficult to detect with traditional methods. Using unsupervised learning, researchers can identify specific groups within alloy data sets that are not simple partitions based on metal compositions, and can help optimise and develop new alloys with customised properties. Incorporating these data-driven methods into alloy design speeds up the discovery process and reveals new connections that were not previously understood, significantly contributing to innovation in materials science. This review outlines the key scientific progress and future possibilities for using unsupervised machine learning in alloy design.

1 Introduction

Materials design has undergone a significant change in recent years, seeing increased adoption of machine learning (ML)[1] to

[a]School of Engineering, Australian National University, Acton, Australia
[b]Faculty of Science, Engineering and Built Environment, Deakin University, Waurn Ponds, Australia
[c]School of Computing, Australian National University, Acton, Australia. E-mail: amanda.s.barnard@anu.edu.au

overcome limitations of empirical methods, which have been principally based on domain expertise and trial-and-error experimentation.[2–4] This has been supported by the availability of large-scale materials data, computational resources and collaboration between the materials, statistics and computer science communities.[5] Machine learning offers a new paradigm for materials design,[6–10] uncovering relationships, patterns and trends that are otherwise obscured in conventional research. By leveraging computational and experimental results, ML models can predict material properties,[11–14] optimise processing

Mr Ninad Bhat is a PhD candidate at the School of Engineering, Australian National University. His research focuses on developing machine learning models for designing aluminium alloys with optimised properties. Before pursuing his PhD, Ninad completed his Bachelor's and Master's degrees from the Indian Institute of Technology Bombay, where he majored in Metallurgical Engineering and Materials Science.

Ninad Bhat

Professor Nick Birbilis is the Executive Dean of the Faculty of Science, Engineering and Built Environment at Deakin University, Australia. His research has sought to rationalise the behaviour of engineering alloys from a deterministic perspective. He has interests including computational studies of materials and machine learning tools to accelerate materials discovery. His awards include the H. H. Uhlig Award, the Australian Academy

Nick Birbilis

of Technological Sciences and Engineering Batterham Medal, along with recognition as a Fellow of ASM International, The Electrochemical Society, International Society of Electrochemistry, NACE (National Association of Corrosion Engineers) and Engineers Australia.

routes,[15,16] and recommend superior material compositions.[17] The integration of ML into materials development not only accelerates the discovery process[18] but enables exploration of material spaces that were previously deemed too complex or computationally expensive to investigate.[19–23]

One of the key strengths of ML is its versatility. A single ML method can be used for multiple tasks, and applied to multiple data sets with entirely different volume, veracity and distributions. Supervised learning techniques are ideal for predictive tasks where historical data can be learned to predict future outcomes.[24,25] These models learn from labelled data sets, where input features are mapped to known outputs, allowing for the prediction of material properties based on compositional and processing variables. This predictive capability is invaluable in the design of alloys,[26] polymers,[27] and nanomaterials.[28–30] By systematically exploring the relationship between input variables and material properties, supervised ML models can guide the design of new materials with optimised characteristics.[31–34] Alternatively, unsupervised learning identifies hidden patterns within data, regardless of the target properties,[35] and can inform new research direction and investments, well in advance of applications. While unsupervised learning is used throughout materials informatics, currently this is an underdeveloped area of metal alloy design, with excellent potential to extract latent knowledge buried in high dimensional combinatorial data. Examples are limited, but include nanoalloys,[36–40] high entropy alloys,[41–58] and industrial Al and Mg alloys discussed in more detail in the coming sections.

1.1 Alloys and applications

Alloys play a crucial role in a wide range of industries, making them essential in most aspects of our modern lives, including

Amanda S. Barnard

Professor Amanda Barnard is the Deputy Director of the School of Computing at the Australian National University, and leader of Computational Science. Her research occupies the intersection of high-performance computing, machine learning, materials science and nanotechnology, focussing on method development addressing small data challenges, (causal) structure–property relationships and explainable AI. She is a Fellow of the Australian Institute of Physics, the Australian Computer Society and the Royal Society of Chemistry. Her awards include the Physical Scientist of the Year from the Prime Minister of Australia, the Frederick White Prize from the Australian Academy of Science, the ACS Nano Lectureship from the American Chemical Society, and the Feynman Prize (Theory) from the Foresight Institute. In 2022 she was appointed a Member of the Order of Australia for services to computational science.

communications, healthcare, transport, infrastructure and our supply of water and electricity. For example, in aerospace,[59] high-strength, lightweight alloys such as aluminium and titanium are essential for constructing aircraft components, where balancing strength and weight is critical.[60] In the automotive industry,[61,62] aluminium alloys are extensively used to reduce vehicle weight and improve fuel efficiency.[62] In construction,[63] steel alloys are utilised due to their durability and load-bearing capacity.[64] In electronics, copper alloys are widely used in electrical wiring and connectors, due to their excellent conductivity and corrosion resistance.[65]

Alloys are materials composed of two or more metallic elements, often combined with non-metallic elements, to enhance their properties compared to their individual components.[66] The primary objective of creating alloys is to achieve superior strength, hardness, fatigue or fracture resistance, corrosion resistance, or other desired characteristics tailored to specific applications.[67] Each alloy is typically defined by the primary component, known as the 'base metal'. In the case of steel, one of the most widely used alloys, the primary components are iron and carbon.[68] The addition of carbon to iron significantly increases the material's strength and hardness, making steel viable for modern construction and manufacturing.[68]

Alloys are further categorised based on their main alloying elements, using a range of internationally recognised numbering systems that reflect industry standards.[69,70] For example, wrought aluminium alloys are divided into eight series (denoted by Nxxx), such as 6xxx (aluminium–magnesium–silicon) and 7xxx (aluminium–zinc) alloys, based on the primary alloying element.[71] Similarly, magnesium alloys are organised into series such as AZ, where aluminium and zinc are the key alloying elements, and AM, where aluminium and manganese are predominant.[71] More information on this numbering system and the alloy designations can be found in ref. 72.

Broadly, there are two main types of alloy: substitutional alloys,[73] where atoms of the alloying element replace atoms of the base metal, and interstitial alloys,[74] where smaller atoms fit into the spaces between the base metal atoms (an exception being a small number of amorphous alloys, that are non-crystalline). Alloys are produced by blending the base metal with the alloying elements. The most common method to achieve this is *via* melting.[75] A molten alloy mixture is then cooled or cast into a solidified structure. Other methods include powder metallurgy,[76] where metals are blended in powdered form and then fused together, and chemical vapour deposition,[77] used for creating thin-film alloys. The production of alloys requires precise control over the composition, temperature, and cooling rate to achieve the desired microstructure.[78] The resulting microstructure of the alloy determines its mechanical and physical properties. This complexity is a significant challenge in alloy design, as even minor variations can lead to substantial differences in performance.

After solidification, further processing is often required to modify the microstructure and enhance the properties of the alloy. Post-solidification processing, termed thermomechanical processing, can also be highly complex. These

processes include rolling,[79] forging,[80] heat-treatment,[71] and solid–state processes that also include controlled quenching[81] (for example, to form martensite in steels) or precipitation hardening[82] (the basis for achieving aerospace aluminium alloys, necessary for aviation).

For these reasons designing alloys is inherently complicated, occupying a vast high dimensional combinatorial design space[71,83,84] where the number of potential multi-component alloys is difficult to explore experimentally. The process of optimising alloys often involves property trade-offs, since enhancing one characteristic, such as strength, can negatively impact another, such as ductility.[85] The growing demand for sustainable materials further complicates alloy design, as it adds the pressure of developing alloys that not only fulfil technical requirements but also minimise environmental impact and cost.[86] To achieve these objectives, traditional alloy design has followed a trial-and-error approach, where the selection of elements and their proportions is guided by the experience and intuition of materials scientists.[82,87] This often involves systematically varying a small subset of alloying element concentrations or processing conditions to achieve the desired properties,[88–90] or rationalising the underlying mechanisms through complex and time-consuming characterisation methods.

2   Research questions

As the demand for new materials with specific properties increases,[86,91] there is a growing need for more efficient and predictive design approaches, that can narrow down the possibilities before attempting to train structure–property models. Conventional methods of alloy development,[92,93] are time-consuming and resource-intensive,[94] and so researchers are increasingly turning to data-driven techniques to address some of the challenges related to traditional materials design processes.[95,96]

Unsupervised learning techniques have emerged as powerful tools in this context, offering the ability to analyse complex, high-dimensional data sets that are common in materials science,[97,98] without the added cost of measuring properties. The objective of unsupervised learning is to identify patterns in an unlabelled data set when no information on the physico-chemical properties is available. Common unsupervised learning tasks include cluster analysis[99] and dimensionality reduction (DR).[100] Cluster analysis involves the grouping of data instances (individual structures) based on their similarities or differences in a high dimensional space using distance metrics. Representative structures (prototypes) can be identified from each cluster centroid. DR involves obtaining lower-dimensional representations of data, which allows simplification and acceleration of model training and improvement in model generalisability. DR includes methods that reduces the number of features needed to describe an alloy, and methods that reduce the number of alloys to the most influential and important subset.[101] These methods enable researchers to uncover hidden patterns, reduce the complexity of data, and identify novel outliers that may correspond to new, previously unexplored materials or properties. Applications of these methods to alloy design are still relatively rare, so there is a considerable untapped opportunity to address important research questions in the field.

2.1   The curse of dimensionality

One of the key challenges in alloy design is the high dimensionality[102] and low volume of data. This results in "curse of dimensionality"[103–105] and makes it difficult to analyse using traditional methods. Dimensionality reduction techniques can address this issue,[84] by reducing the number of independent variables (features), while retaining the essential information. These methods simplify the analysis and help in identifying the underlying patterns in the data set.[106]

2.2   Recognising hidden patterns

The detection of patterns in high-dimensional data is another critical use of unsupervised learning in alloy design.[107] Alloys exhibit complex relationships between composition, processing, and properties, which are often non-linear.[108] Unsupervised learning algorithms, such as clustering and manifold learning, are particularly well-suited for uncovering these patterns without labelling data. Clustering techniques can also group similar data instances based on their features, which can help to focus research.

2.3   Identifying special cases

In virtually every data set, there are special cases that can be useful or detrimental to the training of models and, ultimately, to predictions.[109–111] Examples include archetypes, prototypes, stereotypes, and outliers. Archetypes are the 'pure' instances (on the convex hull), prototypes are the representative instances (or average in high-dimensional space), stereotypes are instances with intrinsic importance (such as thermodynamically stable structures), and outliers are anomalies that can be due to poor sampling, errors in data collection, or rare events. Anomalies can also be caused by defects in the alloys, including microstructural imperfections or processing artefacts.[112] Identifying these defect-related outliers is important for ensuring the quality and reliability of the final alloy produced.[113]

2.4   Structure of the review

This tutorial review has been structured around the unsupervised learning methods used to address these research questions, with sections describing different approaches to dimensionality reduction (Section 3), manifold learning (Section 4), clustering (Section 5), outlier detection (Section 6) and semi-supervised learning (Section 7). These sections contain brief summaries of different methods, highlighting their advantages and disadvantages, and recommended uses in alloy design. Each section concludes with a survey of some previous applications to alloys and alloying metals, to demonstrate the utility and highlight how new knowledge can be gained. To date there are few instances of unsupervised learning of metal alloys and but these applications are

aggregated in Table 1, cross referenced by metals, ML methods and applications. As this area of research is still at an early stage, this review provides a foundation for future studies and complements other reviews covering supervised learning of structure–property relationships.[114-118]

3 Dimensionality reduction

As mentioned above, depending on the number of structural features and chemical features, alloy data sets can be high-dimensional. High-dimensional data is not intuitive for visualisation and produces complicated models that are slow to optimise, train and use in practice. Many different unsupervised algorithms are available to reduce the feature space and improve the efficiency of ML models, the aim of which is to minimise the information loss and maximise the impact of the information retained. Dimensionality reduction methods are applied before ML models are trained, and the most convenient way to evaluate a dimension reduction method is statistically by calculating the Explained Sample Variance (ESV).

The ESV is a quality measure of the deviation between the nth original data instance x_n and the derived data instance $\sum_{j=1}^{k} \alpha_{nj} Z_j$ and is given by:

$$\text{ESV}_i = \frac{\|x_n\|^2 - \|x_n - \sum_{j=1}^{k} \alpha_{nj} Z_j\|^2}{\|x_n\|^2} \tag{1}$$

By evaluating these ESV values, it is possible to state which alloys will be well described by a model. The ESV ranges

Table 1 Previous applications of unsupervised machine learning in metal and alloy research. SOM = self-organizing map; PCA = principle component analysis; UNMAP = uniform manifold approximation and projection; t-SNE = t-distributed stochastic neighbor embedding; AE = autoencoders; ILS = iterative label spreading; LOFA = local outlier factor analysis; RANSAC = random sample consensus. HEA = high entropy alloy

Author	Year	Application(s)	Base metal(s)	ML method(s)	Reference
Sun et al.	2017	Biomedical	Nano Ag	k-Means	119
Syuhada et al.	2018	Chemical analysis	Al, Ti, Cu, Zn	PCA	120
Sun et al.	2018	Biomedical	Nano Ag	SOM	121
Shirinyan et al.	2019	Magnetic applications (sensors, electromagnets)	Fe	SOM	122
Verma et al.	2019	Structural	Fe	t-SNE	123
Jha et al.	2019	Aerospace	Ti, Al, Cr, V	SOM	124
Krishnamurthy et al.	2019	Structural	Fe	t-SNE	125
Verma et al.	2019	Structural	Fe	t-SNE	126
Sun et al.	2019	Biomedical	Nano Ag, Pt	t-SNE, SOM	127
Parker et al.	2020	Electrocatalysis	Nano Pt	ILS	128
Dasgupta et al.	2020	Catalytic design	Single atom alloy	LOFA	129
Tian et al.	2020	Structural	Cu, Zr	RANSAC	130
Parker et al.	2020	Electrocatalysis	Nano Pt	AA	131
Esterhuizen et al.	2021	Catalysis	Rh, Pd, Pt, Ir	PCA	132
Jung et al.	2021	Structural	Fe	AE	133
Liu et al.	2021	Thermal coating	Al	UMAP	134
Esterhuizen et al.	2021	Catalysis	Ir, Pt, Pd, Rh	PCA	135
Subbarao et al.	2021	Aerospace, biomedical	Ti, Al, V	PCA	136
Kim et al.	2021	Structural	Fe	AE	137
Yin et al.	2021	Structural, automobile	HEA	AE	138
Lee et al.	2022	Structural, automobile	HEA	k-Means	139
Chintakindi et al.	2022	Marine	Ni	PCA	140
Lee et al.	2022	Structural, Automobile	HEA	k-Means	141
Xin et al.	2022	Structural	Si	PCA	142
Wenzlick et al.	2022	Structural	Fe	LOFA	113
Bundela et al.	2022	Structural, automobile	HEA	PCA	143
Foggiatto et al.	2023	Sensors	Fe, Ga	PCA	144
Ahmad et al.	2023	Microstructure modelling	Binary Alloy	AE	145
Bhat et al.	2023	Aerospace	Al	ILS	146
Ghorbani et al.	2023	Automobile, electronics	Mg	t-SNE	147
Chen et al.	2023	Biomedical	Al, Ni	UMAP	148
Tiwari et al.	2023	Structural	Al	k-Means	149
Ting et al.	2023	Electrocatalysis	Nano Ru	ILS	150
Roncaglia et al.	2023	Catalysis, biomedical	Ag, Au, Pd, Cu	PCA, k-means	151
Vela et al.	2023	Aerospace	W, Mo, V, Ta, Nb, Al	UMAP	152
Fetni et al.	2023	Microstructure modelling	Binary Alloy	AE	153
Moses et al.	2024	Automobile, electronics	Mg	k-Means	154
Lie et al.	2024	Structural	Fe	t-SNE	155
Usuga et al.	2024	Catalysis	Bimetallic alloys	UMAP	156

between 0 and 1, where 1 is a perfect match. No conclusions should be made for alloys where the ESV is low because these sample instances will be poorly described by a model.

3.1 Feature selection

Feature selection is a crucial preliminary step for reducing the dimensionality of a data set while preserving its most important features.[157,158] The goal is to capture essential information with minimal redundancy, thereby improving the performance and interpretability of models.[159]

Feature selection can be approached through data-driven, domain-driven, and model-driven methods, each with its own focus and advantages. Data-driven feature selection relies on the statistical properties of the data set to eliminate irrelevant or redundant features. For example, when features are highly correlated they provide similar information, so removing one of the correlated features can reduce redundancy without losing valuable information.[160] Similarly, features with low variance across the data set typically contribute little to distinguishing between data instances and can be excluded to simplify the model and reduce noise.[161]

Domain-driven feature selection leverages expert knowledge in alloy design to determine which features are less important or irrelevant. For instance, in alloy data sets, domain experts can choose to remove an element due to its toxicity,[162] thereby focusing the analysis on more significant features. Finally, model-driven feature selection uses insights gained from preliminary modelling to identify the most important features.[161] This approach often involves training a model and assessing which features contribute most significantly to its predictions. For example, certain machine learning models, such as decision trees or random forests, generate feature importance scores[163] that indicate the relevance of each feature to the model architecture. Features with low importance can then be removed, streamlining the model without compromising its performance.

When these methods fail to address the problem, or are inappropriate, transforming the data using feature engineering can help. A survey of feature selection across materials science can be found in ref. 164, and additional examples in ref. 165 and 166.

3.2 Principal component analysis

Principal components analysis (PCA) converts a set of potentially correlated features into a set of linearly uncorrelated variables; the principal components (PCs).[167] PCA takes an $n \times m$ data matrix, X (of n materials and m structural features) and uses an orthogonal linear matrix transformation to express the original data as a linear combination of scores and loadings, described by:

$$X = t^1 p'_1 + t^2 p'_2 + \ldots + t^A p'_A + E = TP' + E \quad (2)$$

where A is the total number of extracted principal components ($A \leq p$) and E is the residual matrix. The new latent variables, t scores, show how the objects relate to each other. The principal components, p, are calculated by operating eigen-

decomposition on the covariance matrix of the data set, and A is determined by retaining a maximal amount of the variance. Typically, the axes of the new coordinate system are oriented to account for maximum variation in the data set. In PCA, the coefficients can be positive or negative, and their sum is not restricted to one.

One of the primary advantages of PCA is its simplicity and computational efficiency, making it ideal for quickly analysing large data sets. Additionally, PCA is deterministic, ensuring consistent results without the variability that can affect other methods described in upcoming Sections of this review. However, PCA is limited to linear transformations and may not effectively capture complex, non-linear relationships in the data (which is often the case with alloy data sets[168]). Additionally, PCA can be heavily influenced by outliers, and in alloy data sets where outliers might indicate unusual material behaviour or errors, this sensitivity can distort results unless managed carefully. Such effects can be minimised by using robust PCA and outlier detection methods in combination.[169] This method has been used widely in materials science for many years.[170] Outlier detection will be discussed in Section 6.

3.3 Singular value decomposition

Singular Value Decomposition (SVD) is another technique used to reduce the dimensionality of the data while preserving its most important features.[171] SVD does this by projecting the original data into a lower-dimensional space that captures the most significant variations. Given a data set represented by a matrix A of dimensions $m \times n$, where m is the number of data instances (*e.g.* number of alloys) and n is the number of features (*e.g.* alloy composition), the SVD of A is defined as:

$$A = U\Sigma V^T \quad (3)$$

where U is an $m \times m$ orthogonal matrix containing the left singular vectors, which represent the principal directions in the data space. Σ is an $m \times n$ diagonal matrix with non-negative singular values σ_i on the diagonal, ordered such that $\sigma_1 \geq \sigma_2 \geq \ldots \geq \sigma_r$, where $r = \min(m, n)$. These singular values quantify the importance of each corresponding singular vector. V is an $n \times n$ orthogonal matrix containing the right singular vectors, which correspond to the principal components in the feature space.

The reduced representation A_k of the original matrix A is given by:

$$A_k = U_k \Sigma_k V_k^T \quad (4)$$

where U_k consists of the first k columns of U, Σ_k is the $k \times k$ diagonal matrix containing the top k singular values, and V_k consists of the first k columns of V.

SVD is effective at separating signal from noise in data, making it particularly valuable for alloy data sets that may contain measurement errors.[172] By focusing on the largest singular values and their corresponding vectors, SVD can significantly reduce the impact of noise, and can be can be adapted to handle missing data,[173] which is especially beneficial

for alloy data sets with incomplete measurements. However, like PCA, SVD is sensitive to outliers and does not capture the non-linear interactions that are crucial in understanding alloy behaviour. SVD has been useful in the processing of images in materials science.[174,175]

3.4 Archetypal analysis

Archetypal analysis (AA),[176] also known as principal convex hull analysis, is a matrix factorisation method that aims to approximate all alloy instances in a data set as a linear combination of extremal points. A given data set of n alloys described by m features is represented by an $n \times m$ matrix, X. Archetypal analysis seeks to find a $k \times m$ matrix Z such that each data instance can be represented as a mixture of the k archetypes. This is achieved by minimizing the residual sum of squares, under some constraints:

$$\text{RSS} = \sum_{i=1}^{n} \left\| X_i - \sum_{j=1}^{k} \alpha_{ij} Z_i \right\|^2 = \sum_{i=1}^{n} \left\| X_i - \sum_{j=1}^{k} \alpha_{ij} \sum_{i=1}^{n} \beta_{ij} X_l \right\|^2 \quad (5)$$

with $\sum_{j=1}^{k} \alpha_{ij} = 1$ with $\alpha_{ij} \geq 0$ and $i = 1, \ldots, n$. and $\sum_{i=1}^{n} \beta_{ji} = 1$ with $\beta_{ji} \geq 0$ and $j = 1, \ldots, k$. The first constraint requires the data to be approximated by convex combinations of the archetypes, whilst the second constraint requires that the archetypes are convex combinations of the data. The resultant archetypes form a convex hull of the data set, but they need not be present in the original set to be identified.

Archetypal analysis provides a set of archetypes that represent the pure types within the data set. Using archetypes of describe a set can make the results more interpretable,[177] since each measured or hypothetical instance is described as a mixture of systems that are easy to understand. However, it is important when using AA that the data is cleaned appropriately, as it uses a least-squares optimisation, which is heavily influenced by the presence of outliers. This approach has been used in nanoinformatics[29] to identify archetypal nanoparticle morphologies.[97,101,178,179]

3.5 Kohonen maps

A Kohonen network,[180] or self-organisation map (SOM), is an unsupervised artificial neural network[181] for non-linearly mapping high-dimensional spaces into low-dimensional spaces, with the advantage of retaining the intrinsic topological relationship of the input data set. SOMs are ideal for visualising multi-dimensional data sets in a single two-dimensional image,[182] and have been recently used to create surface texture maps of metallic nanoparticles suitable for use as material fingerprints.[183]

The basic units of a SOM are neurons which are best organised on hexagonal grids. All neurons can be arranged in a planar (approximate) rectangle, with periodic boundary conditions to connect the upper and lower boundaries and the right and left boundaries so that the SOM plane occupies the surface of a torus. The weights of all neurons are initialised using random numbers. During each training step every neuron competes against all others until each original data instance

finds the one neuron that is closest to it in Euclidean space, referred to as the best matching unit (BMU). Given an input data instance x, and the weight of neuron i, j is w^{ij}, then the Euclidean distance D is:

$$D = \sqrt{\sum_{v-1}^{d} \left(X_v - w_v^{ij} \right)^2} \quad (6)$$

where v is each component of the vector and d is the dimension of the normalised data set. Once the BMU is located, the weights of all neurons centred on it are updated. Initially all neurons on the SOM are updated, until only the BMU is updated at the conclusion of training. This ensures the radius of neighbourhood $\delta(t)$ decreases with each subsequent iteration step, t. In addition to this a linear relation can be adopted with a pre-set maximum number of epochs, n_{epoch}, to train the SOM, such that:

$$\frac{\delta(t) - \delta_0}{t - 1} = \frac{\delta_{n_{\text{epoch}}} - \delta_0}{n_{\text{epoch}} - 1} \quad (7)$$

where δ_0 is the initial radius which has been set to half size of the SOM, $t = 2, 3, 4, \ldots, n_{\text{epoch}}$, and $\delta_{n_{\text{epoch}}}$ is determined by the boundary condition such that it equals one at the last step of training. In addition to decay of the neighbourhood radius, the learning rate $L(t)$ for updating weights on each neuron also decreases with each iteration of t. Weights are updated faster early in the training, and slows toward end of training, based on:

$$\frac{L(t) - L_0}{t - 1} = \frac{L_{n_{\text{epoch}}} - L_0}{n_{\text{epoch}} - 1} \quad (8)$$

where L_0 is the initial learning rate, $L_{n_{\text{epoch}}}$, is the constant and chosen to ensure the training is very fine-grained. As a result, the updating procedure is given by:

$$w^{ij}(t + 1) = w^{ij}(t) + L(t)\exp\left[\frac{-D_x(t)^2}{2\delta^2(t)} \right] \left[x - w^{ij}(t) \right] \quad (9)$$

where $D_x(t)$ is the Euclidean distance of a neuron at i, j from the BMU of x at step t.

One of the key benefits of SOMs is their ability to preserve the topological structure of the data, meaning that alloys with similar properties or compositions will be mapped close to each other on the grid. This topological preservation is particularly valuable when trying to understand relationships and patterns in complex alloy data sets; separating groups that are dissimilar, and the separation distance representing just how dissimilar they are. However, an important consideration in SOM training is the number of epochs, which is a important hyper-parameter. A large number of epochs will result in over-training, leading to a waste of computational resources, but a small number of epochs will result in under-training, and dissimilar alloys may be adjacent in the final SOM, reducing the resolution. It is possible to measure the number of void neurons that have no weight and stop the training when this number stops decreasing over a threshold after, for instance, $n_{\text{epoch}} = 5$, to improve efficiency and autonomy.[184] This has been useful in processing spectroscopic data in materials science.[185–187]

3.6 Autoencoders

Autoencoders are a class of neural networks used primarily for unsupervised learning.[188] Their main objective is to learn a compressed representation (encoding) of input data, which can then be used for tasks such as dimensionality reduction,[189] feature extraction,[190] and anomaly detection.[191]

An autoencoder consists of two main components: an encoder $E(\cdot)$ and a decoder $D(\cdot)$. The encoder compresses the input data x into a lower-dimensional representation z, often referred to as the latent space or code. The decoder then attempts to reconstruct the original input from this compressed representation. The overall structure can be summarised as follows:

$$\text{Encoder: } z = E(x) = f(W_e x + b_e) \tag{10}$$

$$\text{Decoder: } \hat{x} = D(z) = g(W_d z + b_d) \tag{11}$$

$$\text{Reconstruction: } \hat{x} = D(E(x)) \tag{12}$$

where W_e and b_e are the weights and biases of the encoder, with $f(\cdot)$ is a non-linear activation function; and W_d and b_d are the weights and biases of the decoder, with $g(\cdot)$ is another non-linear activation function.

The goal of training an autoencoder is to minimise the difference between the input x and the reconstructed output $\hat{x}$. This difference is quantified by a loss function, typically the mean squared error (MSE):

$$L(x, \hat{x}) = \frac{1}{n} \sum_{i=1}^{n} (x_i - \hat{x}_i)^2 \tag{13}$$

Autoencoders work better in dimensionality reduction in data set non-linear relationships when compared to methods such as PCA.[192] Their flexible architecture allows for task-specific customisation, and they operate without needing labelled data, making them ideal for unsupervised learning scenarios. However, they also come with challenges, such as the need for careful hyper-parameter tuning, potential difficulties in capturing complex data distributions, and a risk of over-fitting, particularly with small data sets.[193] These factors can limit their effectiveness and generalisability in some applications, but they have successfully been applied to materials science problems.[194,195]

3.7 Reducing alloy data

In alloy research, PCA has primarily been used to reduce the feature spaces in prreparation for either clustering[120,196] or training regression models to predict properties.[142] For example, PCA was used to cluster alloy samples using Laser-Induced Breakdown Spectroscopy (LIBS) data.[120] Copper and aluminium presented distinct clusters in the PC plot, as shown in Fig. 1. Brass showed a wide spread in the plot, which could be attributed to the presence of both copper and zinc in high concentrations. However, using LIBS with PCA proved to be a viable method to identify elements in alloys.
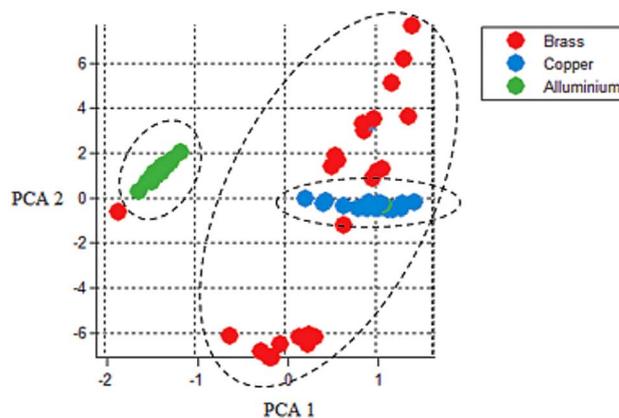

Fig. 1 Principal component plot for Al, Cu, and Brass alloys, demonstrating clear separation between the alloy groups. Reproduced from ref. 197, with permission from Institute of Physics Publishing, Creative Commons Attribution 3.0 licence.

PCA has also been used to reduce the dimensionality of features in molten steel for the prediction of alloying element yield.[142] Using PCA, the features set was reduced such that the cumulative contribution rate of PCs extracted is above 90%, which lead to reduction of dimensions form 16 to 11. These principal components were used as features to train a deep neural network (DNN) to predict alloying yield. The PCA-DNN model demonstrated better performance compared to DNN models trained on the entire feature set, achieving a 0.03 increase in the R^2 score for predicting silicon yield.

Self-organising maps have been used in design of high-temperature Ti alloys and magnetic alloys.[107,124] By using alloy concentrations as input features, SOMs grouped AlNiCo alloys into 64 distinct units.[107] SOM showed a strong correlation between $((BH)_{max}$ and $(BH)_{max}/mass$, as shown in Fig. 2.

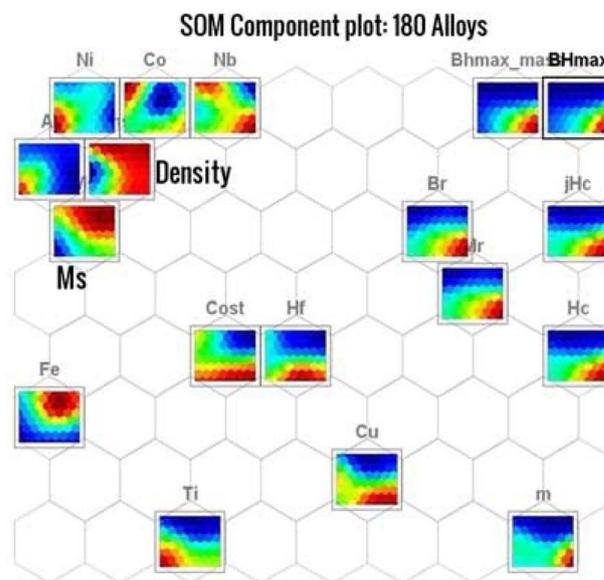

Fig. 2 SOM map showing strong correlations between $((BH)_{max}$ and $(BH)_{max}/mass$, and Br and Mr. Reproduced from ref. 107, with permission from Taylor & Francis, Copyright (2017).

Additionally, studying the variation of magnetic energy density in the maps, it was observed that the top 10 alloys were concentrated in three adjacent units. This proximity suggests a meaningful correlation in the underlying structure of these alloys. SOMs were also used to group Ti alloys, using compositions of equilibrium α-Ti (hexagonal close-packed Ti) and β-Ti (body-centered-cubic Ti) phases calculated through CALPHAD as features.[124]

Archetypal analysis (AA) has been employed in metallic systems to identify seven distinct archetypes in platinum nanoparticles, which were subsequently mapped to seven different nanoparticle within the data set, as illustrated in Fig. 3. Although the application of AA in alloy research remains under-explored, it has been successfully use in materials research to identify unique and special compositions[198] and structures,[178,179,199] providing insights into the underlying patterns within complex data sets. This is a potential area of development for alloys, to reduce the larger sets of hypothetical alloys to the archetypes that may be reflective of particularly application domains.

Autoencoders have been used for feature extraction and dimensionality reduction in the study of alloys.[133,137,138,145,153,200] These models are primarily employed to reduce the

Fig. 4 t-SNE map illustrating spatial gaps in synthetic compositions produced by the diffusion model, highlighting discontinuities in the original compositions. Reproduced from ref. 213, with permission from Springer Nature, Copyright (2024).

dimensionality of microstructural images, transforming high-dimensional data into a lower-dimensional latent space representation. This latent space facilitates the identification of key features essential for understanding the properties of alloys[200] and are also used for training additional machine learning models aimed at optimising microstructures.[133,145,153] The reduced latent space in phase field modelling data was utilised to train an Long Short-Term Memory (LSTM) neural network model for predicting microstructure evolution, resulting in a validation loss of 0.0082.[153]

4 Manifold learning

An alternative way to simultaneously reduce the dimensionality of a high-dimensional alloy data set and visualise the distribution is to use manifold learning. Manifold learning is a non-linear unsupervised approach that generalizes the linear framework of PCA and projects high-dimensional data onto a low-dimensional space.[201] Methods include multidimensional scaling[202] (MDS), locally linear embedding[203] (LLE), isometric mapping[204] (isomap), spectral embedding[205] (SE) and uniform manifold approximation and projection[206] (UMAP). Each have different properties and advantages: SE or MDS ensures data instances near to each other are still close in the low dimensional space; LLE maintains the distance within the local neighbourhood; isomap preserves the geodesic distances between all data; and UMAP can result in better visualisation and significantly faster training than the alternatives. Manifold learning can offer a powerful way of visualising relationships.

4.1 t-Distributed stochastic neighbor embedding

t-SNE has been widely used in materials science due to the inherent tunability that can aid in visualisation.[207] t-SNE groups data instances based on local clustered structure by converting affinities into Gaussian joint probabilities. For n objects x_i in d dimension the t-SNE uses the conditional probability that x_j would be picked as a neighbour given x_i is expressed as:
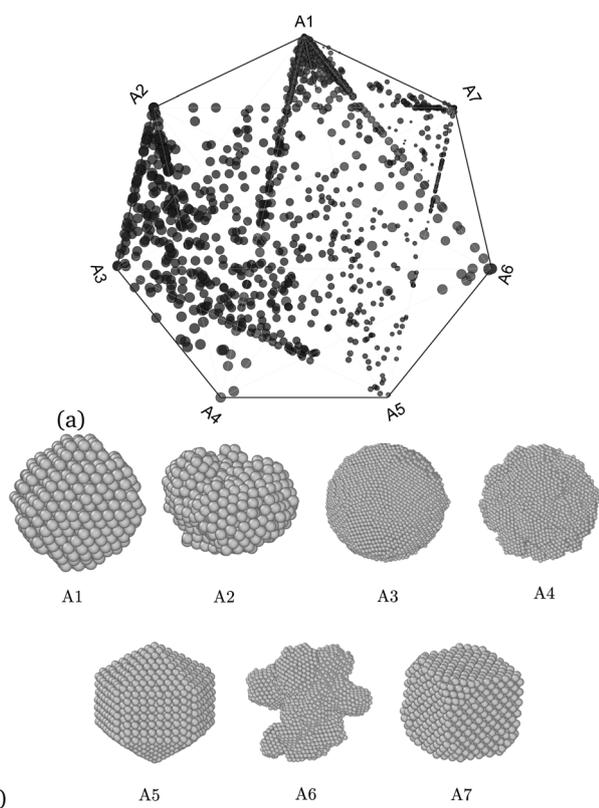

Fig. 3 Example of archetypal analysis of platinum nanoparticle, showing (a) the data distributed with respect to the seven archetypes on a simplex plot (the size of points reflect the relative size of the particles), and (b) the seven nanoparticles in the data set closest matched archetypes. Reproduced from Reference with permission from Institute of Physics Publishing (IOPP), Copyright (2020).
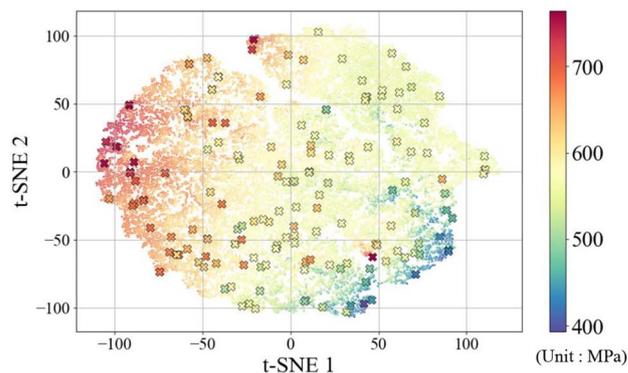
$$P(x_j|x_i) = \frac{\exp\left(-\|x_i - x_j\|^2 \big/ 2\sigma_i^2\right)}{\sum\limits_{k \neq i}\exp\left(-\|x_i - x_k\|^2 \big/ 2\sigma_i^2\right)} \qquad (14)$$

where σ_i is the variance of the Gaussian that is centred on x_i. σ_i is adapted to the density of the data such that smaller values are used for data in high density. The joint probabilities in the high-dimensional space is then set as:

$$P(x_i, x_j) = \frac{P(x_j|x_i) + P(x_i|x_j)}{2n} \qquad (15)$$

For the low-dimensional counterparts, y_i of the high-dimensional data x_i, a Student t-distribution with a degree of freedom one is used to compute the joint probabilities $Q(y_i, y_j)$ as:

$$Q(x_i, x_j) = \frac{\left(1 + \|y_i - y_j\|^2\right)^{-1}}{\sum\limits_{k \neq i}\left(1 + \|y_i - y_k\|^2\right)^{-1}} \qquad (16)$$

This distribution is heavy-tailed so that dissimilar objects in low-dimensional space can be modelled even if they are far apart. The optimisation objective is to equate $P(x_i, x_j)$ and $Q(x_i, x_j)$, which means minimising the cost function $\sum_{i \neq j} P_{i,j} \log(P_{i,j}/Q_{i,j})$.

By tuning the t-SNE hyper-parameters to achieve a clear visualisation suitable for qualitative assessment, and then encoding the distribution of the structural features and property labels using different colours, fast and intuitive relationships can be discerned without extensive training and evaluation of machine learning models.[208] However, while t-SNE excels at preserving the local structure, it often struggles to maintain the global structure of the data, which can lead to misleading distances between clusters and an inaccurate reflection of relationships in the high-dimensional space.[209] Additionally, t-SNE is non-deterministic,[210] meaning that different runs on the same data can produce slightly varying visualisations, which can be confusing and pose challenges for reproducibility.

4.2 Uniform manifold approximation and projection

UMAP is popular technique that has ability to preserve both the local and global structure in high-dimensional data.[211] UMAP starts by constructing a weighted graph G where each point x_i is connected to its nearest neighbours based on a distance metric. The weight w_{ij} between points x_i and x_j is computed using a fuzzy membership function:

$$w_{ij} = \exp\left(-\frac{d(x_i, x_j) - \rho_i}{\sigma_i}\right) \qquad (17)$$

where $d(x_i, x_j)$ is the distance between x_i and x_j, ρ_i is the distance to the nearest neighbour of x_i, and σ_i is a scaling parameter that determines the smoothness of the local fuzzy simplicial set.

The global weighted graph is then formed by combining the local fuzzy simplicial sets. This is achieved by taking the union of all local graphs and symmetrising the edge weights:

$$w_{ij} = w_{ij} + w_{ji} - w_{ij} \cdot w_{ji}. \qquad (18)$$

UMAP finds a low-dimensional representation $Y = \{y_1, y_2, \ldots, y_n\}$ of the data set by minimizing the cross-entropy between the fuzzy simplicial sets in the original high-dimensional space and the low-dimensional space. The objective function for optimisation is:

$$\mathscr{L} = \sum_{i \neq j} w_{ij}\log\left(\frac{w_{ij}}{\hat{w}_{ij}}\right) + (1 - w_{ij})\log\left(\frac{1 - w_{ij}}{1 - \hat{w}_{ij}}\right) \qquad (19)$$

where $\hat{w}_{ij}$ is the corresponding edge weight in the low-dimensional space.

UMAP is deterministic by default, ensuring consistent results for the same data and parameters, which significantly enhances reproducibility.[211] UMAP performs better than t-SNE in preserving global structure,[212] but still requires careful tuning of hyper-parameters, such as the number of neighbours and minimum distance, to achieve optimal results for different data sets.

4.3 Manifold learning of alloys

t-SNE is primarily used in alloy design for visualising feature distributions in a two-dimensional space, and for training regression models using the reduced features.[147,148,213] For example, t-SNE was applied to visualise synthetically generated data from a diffusion model for Al 7xxx alloys revealing distinct groups reflecting dissimilar materials in the original high dimensional space (as shown in Fig. 4). These were attributed to the uneven elemental distribution in the original CU data set (the acronym referring to the set consisting of alloy compositions, without the corresponding elemental properties) used for the diffusion model.[213] In Mg alloys, t-SNE was also used to project data into 2-dimensional spaces, followed by clustering using the BIRCH algorithm,[214] which identified seven distinct clusters.[147] t-SNE was also used in a separate study to reduce the dimensionality of an alloy data set, with the reduced dimensions serving as features for k-Means clustering to discover new steel groupings with distinct mechanical properties, particularly regarding ultimate tensile strength (UTS) across various temperature ranges.[215] Additionally, t-SNE has been applied to dimensionality reduction where the reduced features were subsequently used to train regression models for predicting endpoint carbon content in steels, achieving an accuracy of 0.975, which exceeded the 0.917 accuracy of models trained without t-SNE feature reduction.[216]

Similarly, UMAP has successfully applied to alloy data sets.[134,148,153,156,217] In high-entropy alloys (HEAs), UMAP was employed to visualise the distribution of the test feature set relative to the training feature set in a 2D space,[217] as illustrated in Fig. 5. This visualisation revealed that the poorer-performing test set instances were located further from the training data instances, highlighting a potential discrepancy between the training and test sets, akin to a type of post-hoc forensic analysis. UMAP was used to project the composition of quasicrystals into a 2D space to investigate potential biases in the distribution of various stable quasicrystal compositions.[129] However, no
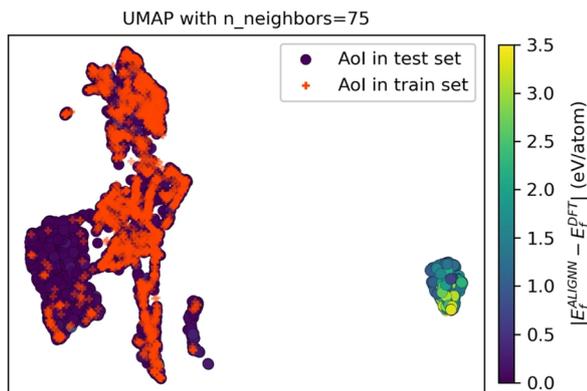
Fig. 5 UMAP projection of the 90-dimensional feature space for both AoI training and test sets, highlighting that test samples with poor predictions are positioned outside the regions covered by the training data. Reproduced from ref. 217, with permission from Nature Publishing Group, Creative Commons Attribution 4.0 International License.

biases were found between stable quasicrystals, approximant crystals, and ordinary crystals. UMAP was also used to project a high-dimensional HEA design space into two dimensions, facilitating the visualisation of relationships between alloy compositions and their properties.[152] By applying property constraints, such as melting temperature or yield strength, UMAP visualisations helped filter the feasible design space for alloys, which was later validated using density functional theory simulations. In AlN thin-film, UMAP has been used for dimensionality reduction of the feature set, which was then used to train a CatBoost model to predict residual stress.[148]

5 Clustering

Clustering involves grouping data instances into clusters based on similarity in a high dimensional feature space. In general, clustering has become an important part of materials informatics, finding use in a numerous application domains.[218–221] A variety of clustering algorithms exist, each tailored to specific types of data and application contexts, and they differ in terms of scope, efficiency, and prerequisites.[222] The choice of a clustering algorithm often depends on the subjective definition of what constitutes a cluster in a given scenario, as different models offer unique perspectives on the data set.[223,224] Clustering models can be categorised as: centroid based,[225] distribution based,[226] density based,[227] connectivity based[228] (*e.g.* hierarchical clustering), graph based[229] and affinity based.[230] In addition to these definitive cases, where each data instance can only belong to one cluster, there are also clustering models where a given observation can contribute to more than one cluster (weighted accordingly).[231]

5.1 Centroid-based

Centroid-based clustering is a method where clusters are represented by central points, known as centroids, that ideally minimise the distance between data instances and their respective cluster centres.[232] A well-known example of centroid-based clustering is *k*-Means,[233] which assumes that each of the *k*

clusters can be represented by a single centroid $c_k \in \mathbb{R}^d$, which identifies a local optimum for minimising the sum of squared error (MSE). The MSE optimises for spherical and "compact" clusters, which means that *k*-Means suffers from only identifying convex-shaped clusters, such that a convex set C is contained in the data set X has m elements if for all non-negative real-numbers $w_1, \ldots, w_m$ such that $w_1 + \ldots + w_m = 1$, when $w_1 x_1 + \ldots + w_m x_m \in X$ then the $w_1 x_1 + \ldots + w_m x_m \in C$.

k-Means is favoured for its simplicity, computational efficiency, and scalability, making it particularly useful in alloy design. The interpretability of *k*-Means results, with each cluster represented by a centroid, also aids in understanding the underlying structure of alloy data. However, this method comes with limitations, particularly its assumption of convex and similarly sized clusters. Additionally, *k*-Means is sensitive to the initial choice of centroids, which can lead to inconsistent clustering outcomes, and it struggles with clusters of varying sizes and densities, common in diverse alloy systems.

5.2 Distribution-based

Distribution-based clustering assumes that the data instances are generated from a mixture of underlying probability distributions.[234] The goal is to identify these distributions and assign each instance to the distribution it most likely belongs to. One of the most commonly used distribution-based clustering methods is the Gaussian Mixture Model (GMM),[235] which is a probabilistic model that assumes that the data is generated from a mixture of several Gaussian distributions, each with its own mean and variance. The overall model is a weighted sum of these Gaussian distributions, which are estimated using the Expectation-Maximization (EM) algorithm.[236] The probability density function (PDF) for each instance x_i in a data set $X = \{x_1, x_2, \ldots, x_n\}$ is given by:

$$P(x_i) = \sum_{j=1}^{k} \pi_j \cdot \mathcal{N}(x_i | \mu_j, \Sigma_j) \tag{20}$$

where π_j is the weight (or mixing coefficient) of the jth Gaussian component, with $\sum_{j=1}^{k} \pi_j = 1$, and $\mathcal{N}(x_i | \mu_j, \Sigma_j)$ is the Gaussian distribution with mean μ_j and covariance matrix Σ_j, defined as:

$$\mathcal{N}(x_i | \mu_j, \Sigma_j) = \frac{1}{\sqrt{(2\pi)^d |\Sigma_j|}} \exp\left(-\frac{1}{2}(x_i - \mu_j)^T \Sigma_j^{-1} (x_i - \mu_j) \right) \tag{21}$$

where d is the dimensionality of the data.

The EM algorithm is used to estimate the parameters $\{\pi_j, \mu_j, \Sigma_j\}_{j=1}^{k}$ using Expectation (E) and Maximization (M) steps. In the E step, the algorithm calculates the likelihood of each data instance belonging to each cluster based on the current model. In the M step, it updates the cluster parameters (such as the importance of each cluster, the centre of each cluster, and how spread out each cluster is) based on these calculated likelihoods. These steps are repeated until the model's parameters stabilise and no longer change significantly.

GMMs offer several advantages in alloy design due to their flexibility in modelling complex clusters and providing

probabilistic assignments of data instances to clusters. This approach is particularly useful when dealing with overlapping phases or heterogeneous data, as it allows for a more nuanced representation of cluster memberships. However, the method also comes with drawbacks, including its computational complexity, especially when dealing with large or high-dimensional data sets. Additionally, GMMs are sensitive to the initialisation of parameters, which can lead to convergence on local optima rather than the global optimum. Moreover, the assumption that the underlying data follows a Gaussian distribution may not always be valid in alloy design. If the actual data distribution deviates significantly from a Gaussian distribution, this could lead to poor model performance.

5.3 Density-based

Density-based methods are particularly adept at discovering clusters of arbitrary shapes, making them well-suited for complex materials systems where the distribution of data instances can be highly irregular.[234] The most well-known density-based clustering algorithm is DBSCAN (Density-Based Spatial Clustering of Applications with Noise),[237] which relies on two key parameters: ε (epsilon), which represents the maximum distance between two points for one to be considered in the neighbourhood of the other, and MinPts, the minimum number of points required to form a dense region, or cluster. The algorithm begins by identifying core instances with the least MinPts points within a radius of ε. The neighbourhood of p is defined as:

$$N_\varepsilon(p) = \{q \in D | \text{dist}(p, q) \leq \varepsilon\} \quad (22)$$

where D is the data set and $\text{dist}(p, q)$ is the distance metric, typically Euclidean. An alloy q is directly density-reachable from p if $q \in N_\varepsilon(p)$ and p is a core point. Further, q is density-reachable from p if there is a chain $p_1, p_2, \ldots, p_n$ where $p_1 = p$ and $p_n = q$, such that each p_{i+1} is directly density-reachable from p_i.

Two instances p and q are density-connected if there is an instance o such that both p and q are density-reachable from o. The clustering process in DBSCAN starts with an arbitrary p and retrieves all instances that are density-reachable from p. If p is a core point, a cluster is formed. If p is a border point, no points are density-reachable from p, and p is labelled as noise or an outlier. The algorithm continues to iterate over all instances in the data set, forming clusters by merging density-connected components.

Density-based clustering, particularly DBSCAN, offers significant advantages due to its ability to discover clusters of arbitrary shapes and sizes. It is also effective at handling noise and outliers, which are common in experimental alloy data sets. DBSCAN does not require the number of clusters to be specified beforehand, making it suitable for exploratory data analysis. However, DBSCAN has its limitations, including its sensitivity to the choice of parameters (ε and MinPts), which can significantly impact the clustering outcome. Additionally, DBSCAN may struggle with varying densities within the same data set,

which can lead to the merging of clusters with different densities or the failure to identify some clusters altogether.

5.4 Connectivity-based

Hierarchical clustering algorithms are connectivity-based and identify a systematic hierarchy of cluster labels for a data set, such that there are l layers in the hierarchy, where l is the number of data instances. Hierarchical clustering is either divisive or agglomeration,[238] with divisive methods breaking down large clusters into smaller ones,[239] and agglomerative methods building up small clusters into larger ones.[240] Agglomerative clustering begins by assigning each instance as an individual cluster and recursively merges them until all data instances are in the same cluster, based on their relative distance in the high dimensional feature space, effectively producing a cluster-tree. The pair of clusters with the smallest distance are merged, with the distance defined with linkage criteria, such as single, average, complete or Ward linkage. An advantage of hierarchical clustering is that the number of clusters, K, does not need to be known in advance. However, the time complexity is high and scales quadratically with the number of instances, N.

Ward clustering, also known as Ward's method, is a hierarchical, agglomerative clustering technique that minimizes within-cluster variance by iteratively merging clusters that result in the smallest increase in total variance.[241] One of the key strengths of Ward clustering is its tendency to produce clusters of approximately equal size, which can be beneficial in applications where balanced groupings are desired. Additionally, because it focuses on minimizing variance, Ward clustering often yields more compact and well-defined clusters compared to other hierarchical methods.[242] However, Ward clustering is computationally intensive, especially for large data sets, because it requires the calculation of distances between all pairs of data instances at each step.[243]

Connectivity-based clustering, particularly hierarchical clustering, is more interpretable than the alternative, as it allows researchers to see relationships in the data at different levels of detail. While hierarchical clustering can be computationally demanding, this is less of an issue for alloy data sets, which are typically not very large. However, the results can vary depending on the chosen linkage method, which can affect how the clusters are formed.

5.5 Graph-based

Graph-based clustering is used when the structure of data can be represented as a network of interconnected points. In graph-based clustering, the data is represented as a graph $G = (V, E)$, where V is a set of vertices (nodes) corresponding to the data instances, and E is a set of edges that represent the relationships or similarities between these points. The weight of an edge typically indicates the strength of the relationship, with higher weights signifying stronger similarities. The goal of graph-based clustering is to partition the graph into subgraphs or clusters such that the nodes within each cluster are more densely connected to each other than to nodes in other clusters. This results in groups of data instances that are highly similar

© 2024 The Author(s). Published by the Royal Society of Chemistry

or related according to the graph structure. Common graph-based clustering methods include Spectral Clustering,[244] Minimum Spanning Tree (MST) clustering,[245,246] and Highly Connected Subgraphs (HCS).[229]

Spectral clustering[244] is one of the most widely used graph-based algorithms. It uses a spectrum of eigenvalues of the similarity matrix as a quantitative assessment of the relative similarity of each pair of points in the data set, even if the input is not a graph. The similarity matrix may be defined as a symmetric matrix A, where $A_{ij} \geq 0$ measures the similarity between instances i and j. Clustering is applied to the eigenvectors of a Laplacian matrix of A, using the smallest eigenvalues that meet this condition. Spectral clustering is particularly useful for non-convex data or when data can not easily be described by the location of the centroid and the size, shape and density of the surrounding data instances.

Spectral clustering is highly effective for identifying clusters in data that are non-convex or irregularly shaped, where traditional methods like k-Means may fail. By operating in a reduced-dimensional space, it can reveal the underlying structure of the data that might not be apparent in the original feature space. However, the method has some drawbacks, including its computational intensity, especially in the eigenvalue decomposition step, which can be challenging for very large data sets. Additionally, spectral clustering requires a well-defined similarity matrix, and the quality of clustering results heavily depends on how this matrix is constructed. Choosing the right parameters for the similarity matrix can be non-trivial and may require domain-specific knowledge.

5.6 Evaluating clustering results

Evaluating clustering results can be challenging due to the absence of a ground truth, but it is an important step to ensure the predictions are reliable. One of the most convenient ways of doing this is to calculate the ESV,[247] as described above, but there are a number of other metrics available to evaluate the performance of clustering algorithms. The silhouette score (S, or silhouette coefficient)[248] is a metric used to calculate the consistency of a clustering result, reported in the range from -1 to 1, such that for each data instance:

$$S = \frac{L - M}{\max(M, L)} \quad (23)$$

where M is the average intra-cluster distance, L is the average inter-cluster distance, and S is the silhouette coefficient of the data instance. The silhouette score for the data set S is then obtained as the average silhouette coefficient over all data instances. This score measures how similar an instance is to its own cluster, and higher is always better. Clear and well-separated clusters have $S \approx 1$; similar or poorly separated clusters have $S \approx 0$; and clusters with incorrectly assigned instances have $S \approx -1$. The silhouette score can be calculated with any distance metric, such as the Euclidean distance or the Manhattan distance.

The Davies–Bouldin score (DB)[249] is defined as the average similarity measure of each cluster with its most similar cluster,

reporting values greater than 0, where similarity is expressed as the ratio of within-cluster distances to between-cluster distances, such that:

$$DB = \frac{1}{K} \sum_{i=0}^{K} \max_{j \neq i} \frac{m_i + m_j}{M_{i,j}} \quad (24)$$

where K is the number of clusters, $M_{i,j}$ is the separation between clusters i and j, and m is the within-cluster scatter. The score is constrained to be symmetric and non-negative, but no cluster must be similar to another. Clusters that are well separated and less dispersed will result in a lower, and therefore better, score.

The Calinski–Harabasz score (CH, also referred to as the Variance Ratio Criterion, VRC)[250] evaluates the optimal number of clusters based on the variance, such that:

$$CH_K = \frac{\sum_{i=1}^{K} N_i \|n_i - n\|^2}{\sum_{i=1}^{K} \sum_{x \in c_i} \|x - n_i\|^2} \times \frac{N - K}{K - 1} \quad (25)$$

where K is the number of clusters, N is the number of instances, n is the mean of the sample data, n_i is the centroid of cluster i, x is an instance, and k_i is the ith cluster. The modula are the L^2 norms that can be calculated with the Euclidean distance. Well-defined clusters have a large inter-cluster variance and a small intra-cluster variance, so the optimal number of clusters maximises Calinski–Harabasz value.

An alternative way to evaluate clustering outcomes is to use a semi-supervised method such as iterative label spreading, as discussed in Section 7.1.

5.7 Clustering in alloy design

Clustering methods have been used to uncover underlying patterns in a m number of alloy data sets.[139,141,149,154,251] In Al6xxx alloys, the k-Means algorithm was used for clustering data following feature reduction via PCA,[149] leading to the identification of five distinct groups (as shown in Fig. 6). The impact of feature variations within these clusters on the alloys' properties was analysed using model-agnostic explanation methods, such as the LIME algorithm.[253] This analysis revealed a negative influence of the Mg : Si ratio on mechanical properties, attributed to the formation of Mg_2Si precipitates. This relationship would have been obscured during a general regression analysis.

In a Mg alloys corrosion data set, k-Means clustering produced more distinct and separable clusters compared to affinity propagation and hierarchical clustering, as evaluated by scoring metrics such as the silhouette score, Calinski–Harabasz index, and Davies–Bouldin index.[154] The k-Means algorithm identified 8 clusters within the data set. Further analysis revealed that two of these clusters were characterised by high I_{corr} and E_{corr} values. Specifically, Fe was found to contribute to corrosion in the alloys of cluster 1, while the presence of Cl was identified as a contributing factor to corrosion in cluster 2. Once again, while a general regression analysis may have uncovered these underlying factors, the clustering is instrumental in
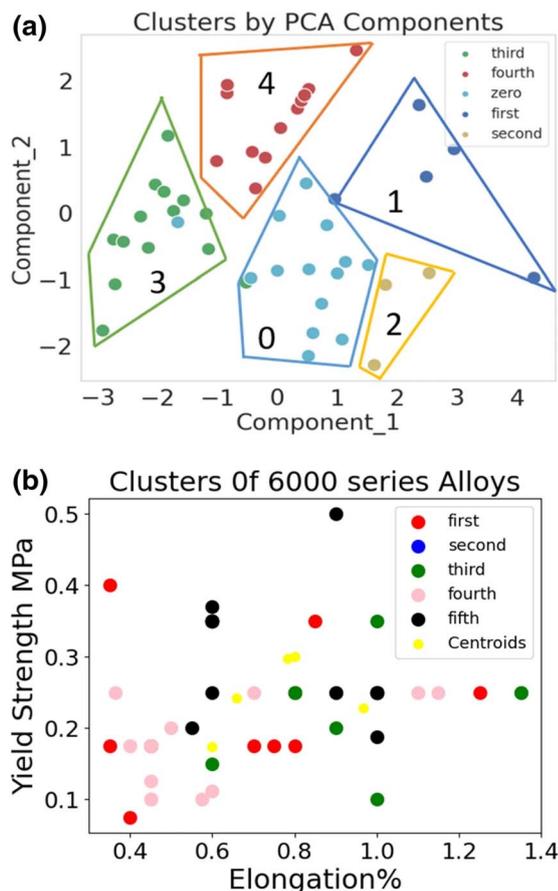
Fig. 6 k-Means clustering with PCA (a) and without PCA (b). The plot in (a) demonstrates the benefits of combining k-Means with PCA, resulting in more distinct clusters compared to using k-Means alone. Reproduced from ref. 252, with permission from Springer Nature, Creative Commons Attribution 4.0.

Fig. 7   Dendrogram illustrating the hierarchical clustering of features used in predicting stacking fault energies in high entropy alloys. Reproduced from ref. 255, with permission from Elsevier, Copyright (2023).

showing that they are likely separate mechanisms affecting different alloys rather than simply two influential base metals.

k-Means clustering was used to analyse local variable attributions in the phase classification of multi-principal element alloys (MPEAs) using a support vector machine.[139,141] Notably, cluster-specific feature importance differed significantly from global feature importance. This distinction is crucial because relying solely on global importance can obscure variables that are critical for predicting specific phases, potentially leading to misleading conclusions in multi-class classification tasks. Integrating cluster-specific insights ensures a more accurate and targeted MPEA design.

Other clustering algorithms have seen more limited use in alloy design. DBSCAN has been applied to cluster Kinetic Monte-Carlo simulation data of Al–Sc alloys, effectively identifying Sc atoms not belonging to precipitates as outliers, which were then removed before further analysis.[254] The dendrogram resulting from the hierarchical clustering of HEAs, illustrated in Fig. 7, highlighted that stacking fault energy (SFE) is strongly influenced by the Rule of Mixtures (RoM) values for formation enthalpy, density, and electronegativity.[255] Graph-based clustering methods, such as spectral clustering, have not yet been applied to alloy design. However, they have been effectively utilised to cluster polymers.[256–258] For example, spectral clustering successfully identified meta-stable and transition states in polymer molecular dynamics simulations. A similar approach could be employed in alloy research to identify meta-stable precipitates. Other potential applications in alloy research include microstructure analysis and the identification of compositional clusters.

6   Outlier detection

Outlier detection is used to identify data instances that deviate significantly from the majority of the data. These outliers can provide crucial insights, reveal errors,[259] or indicate novel phenomena.[260] An outlier is an observation that lies at an unusually large distance from the central tendency or distribution of other values in a data set.[261] If x_i is a data instance and μ and σ represent the mean and standard deviation of the data set, respectively, then an outlier is typically defined as a data instance where the distance $|x_i - \mu|$ exceeds a threshold, such as $k\sigma$, where k is a constant:

$$|x_i - \mu| > k\sigma \tag{26}$$

Outliers can be classified into three types: global outliers (also known as point outliers),[262] which deviate significantly from the rest of the data set; contextual outliers,[263] which are considered outliers in a specific context but not necessarily in the general data set; and collective outliers,[261] which are a collection of data instances that collectively deviate from the rest of the data set, even if individual points within the group may not be outliers.
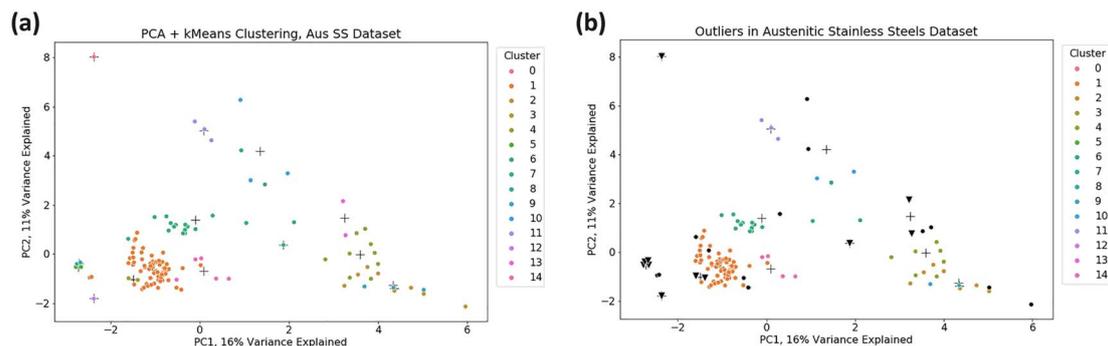
Fig. 8 Visualisation of the two largest principal components of the austenitic stainless steel data set with k-Means clustering applied, indicated by crosses representing cluster centres. (b) Outliers in the data set are detected using two approaches: the z-score method. Reproduced from ref. 113, with permission from Springer Nature, Copyright (2022).

The detection of outliers involves different techniques depending on the type of outlier. Global outliers are typically identified using statistical methods, such as z-scores[264] or Tukey's fences,[265] which flag data instances that significantly deviate from the mean or median. Contextual outliers require understanding the specific context or conditions that define normal behaviour; they are often detected using techniques like clustering[266] or time-series analysis,[267] or methods such as RANSAC (Random Sample Consensus),[268] which iteratively fits models to subsets of the data and identifies outliers as those points that do not conform to the best model. Collective outliers are more complex and are usually detected through density-based methods,[269] or graph-based approaches,[270] which analyse the relationships and collective behaviour of data instances.

6.1 Outlying alloys

ML-based outlier detection methods have been employed to identify shear transformation zones (STZs) in amorphous alloys, which are challenging to detect experimentally due to their transient nature.[130] Among the methods tested, linear RANSAC proved to be the most accurate in identifying these outliers.

Unsupervised learning techniques have also been applied to identify outliers, as shown in Fig. 8, in data sets of ferritic-martensitic steels and austenitic stainless steels.[113] Initially, the data set was clustered using PCA and the k-Means algorithm. Outliers were then identified using the Z-score, calculated as:

$$Z = \frac{X - \mu}{\sigma} \tag{27}$$

where X is the value of the data instance, μ is the mean of the cluster, and σ is the standard deviation. Additionally, clusters with a low number of alloys were considered as outliers. Removing these outliers before training a regression model to predict creep life resulted in a 0.037 increase in test set accuracy compared to a model trained without outlier removal. While the decision to remove outliers can be hard when confronted with small data sets of alloys that were difficult and/or expensive to produce, this step also increases robustness of the model by

eliminating localised under-fitting in regions of the feature space that are poorly represented. This is particularly important in metallurgical industries such as additive manufacturing.[271–273]

7 Semi-supervised learning

Semi-supervised learning (SSL) is a machine learning field that combines supervised and unsupervised learning.[274] It uses a small amount of labelled data alongside a larger pool of unlabelled data to improve model performance. The core idea behind SSL is that unlabelled data, when combined with a small amount of labelled data, can greatly improve the learning process.[275] SSL works on the assumption that the unlabelled data contains useful information about the structure of the data distribution, which can help improve the accuracy of predictions.[274] Several methods are used in SSL, such as self-training, where the model labels unlabelled data and retrains itself; co-training, which involves multiple models working together to label the data; and graph-based methods, which use the relationships between data instances to spread labels across the data set. This approach is particularly valuable when labelling data is costly or time-consuming, as is often the case in materials science.[276,277]

7.1 Iterative label spreading

Iterative label spreading (ILS)[278] is a semi-supervised clustering algorithm, based on a general definition of a cluster and the quality of a clustering result, and is capable of predicting the number and type of clusters and outliers in advance of clustering, regardless of the complexity of the distribution of the data.[131,279,280] ILS can be used to evaluate the results from other clustering algorithms or perform clustering directly. It has been shown to be more reliable than alternative approaches for simple and challenging cases (such as the null and chain cases) and to be ideal for studying noisy data with high dimensionality and high variance, as is typical for alloys.

Direct clustering is achieved using this algorithm by initializing one labelled instance and applying ILS to obtain the ordered minimum distance ($R_{\min}(i)$) plot, as described in detail in ref. 279. The number of clusters can be automatically
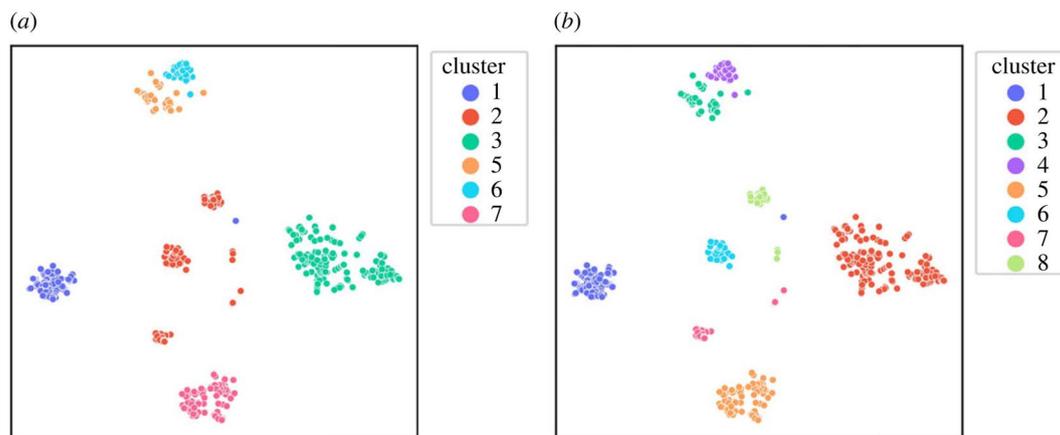
Fig. 9 Identification of clusters using Iterative Label Spreading (ILS): (a) clusters identified during the first iteration of ILS, and (b) clusters identified during the second iteration of ILS applied to each sub-cluster. Reproduced from ref. 145, with permission from Royal Society, Creative Commons Attribution License.

extracted by identifying peaks in the $R_{\min}(i)$ plot (due to density drops between clusters) that divide the plot into n regions. This can be automated using a continuous wavelet transform peak finding algorithm with smoothing over p points. The smoothing essentially sets the minimum cluster size to identify clusters of no smaller than p. Alternatively, if clear peaks are present, they can be identified easily by visual inspection. One instance can be relabelled in each region (preferably in a dense region, *i.e.* several grouped minima) to run ILS again and obtain a fully labelled data set with n clusters defined. ILS can also be applied to each individual cluster to confirm that each region is a single cluster that should not be divided further.

7.2 Semi-supervised learning of alloys

ILS has previously been applied to both metallic particles and Al6xxx alloys. It has been used to distinguish between two separable clusters in Pt nanoparticles, with one cluster comprising exclusively disordered nanoparticles and the other containing only ordered nanoparticles.[128] In aluminium alloys ILS identified six clusters, as illustrated in Fig. 9a, and was then able to identify further sub-clusters on a second pass, as depicted in Fig. 9b. On analysing the alloys within these clusters, it was observed that their mechanical properties varied within certain ranges. This suggests that specific clusters could be used for optimisation when the target mechanical properties are known. The clusters were subsequently demonstrated to be separable classes using a decision tree classifier.[281] The novel classes identified through ILS were then used to enhance the accuracy of forward predictions by training class-specific regressors.[282] Further optimisation with these class-specific regressors led to improved aluminium alloy designs compared to a class-agnostic approach.[283] Applying similar workflows to other alloy systems remains an area for future investigation.

8 Summary and opportunities

This brief review suggests that the use of unsupervised methods in alloy design is on the rise, but researchers may not be taking full advantage of these methods. To date the majority of unsupervised learning for alloy design has focused on preparing the data for more effectively supervised learning (such as transforming elemental features into principle components), or capturing established domain knowledge (such as visualising distributions using manifold learning). With the increase in data available, there are more opportunities to use unsupervised machine learning methods than supervised learning, without the added expense of measuring properties. While machine learning is currently widely employed for tasks such as dimensionality reduction and clustering, the community has yet to venture beyond the most simple approaches. Manifold learning, outlier detection, and semi-supervised learning are all under-explored. This presents significant opportunities for further research and innovation in these areas.

Based on this summary, research in alloy design should focus on exploring the use of more sophisticated methods to identify deeper relationships between alloys before moving to property prediction or inverse design.[145,162] Recent research has demonstrated that the use of clusters identified through ML can partition the data into more predictable groups and significantly improve the accuracy of the model for aluminium alloys.[282] Optimising alloy design within smaller clusters is a more sustainable approach compared to optimising alloys in the entire search space, as it reduces redundancy and focuses the models on metals and characteristics that have greater utility in the domain. Additionally, future opportunities also include enhancing data integration and diversity, using a broader range of alloy compositions and processing conditions; and development of advanced unsupervised algorithms specifically tailored for the complexities of alloy systems. This includes algorithms capable of handling multi-scale[284] and multi-modal data,[285] as well as those that can better capture the non-linear relationships and high-dimensional interactions that characterise alloy behaviour. The emergence of novel methods in computer science will also open up new opportunities, including unsupervised representation learning[286] (evidenced by the rise of large language models[287]), deep clustering

algorithms that use neural networks to learn latent representations of data that improve cluster assignment, graph-based unsupervised learning[288,289] and unsupervised domain adaptation[290] using methods in adversarial learning.[291] Self-supervised learning could bridge the gap between supervised and unsupervised learning,[292–294] by leveraging methods such as contrastive learning which focuses on learning by comparing data samples.[295–297] There is also the potential of exploring hybrid models that combine unsupervised learning with other approaches to further enhance discovery and optimisation processes in alloy design.

Data availability

No data was generated or used as part of this review.

Conflicts of interest

There are no conflicts of interest to declare.

Acknowledgements

Notes and references

1 S. Ramakrishna, T.-Y. Zhang, W.-C. Lu, Q. Qian, J. S. C. Low, J. H. R. Yune, D. Z. L. Tan, S. Bressan, S. Sanvito and S. R. Kalidindi, *J. Intell. Manuf.*, 2018, **30**, 2307–2326.

2 G. R. Schleder, A. C. M. Padilha, C. M. Acosta, M. Costa and A. Fazzio, *J. Phys.: Mater.*, 2019, **2**, 032001.

3 D. Morgan and R. Jacobs, *Annu. Rev. Mater. Res.*, 2020, **50**, 71–103.

4 B. Lu, Y. Xia, Y. Ren, M. Xie, L. Zhou, G. Vinai, S. A. Morton, A. T. S. Wee, W. G. van der Wiel, W. Zhang and P. K. J. Wong, *Advanced Science*, 2024, **11**, 2305277.

5 H. Durrant-Whyte, *Nat. Rev. Mater.*, 2021, **6**, 641.

6 T. Zhou, Z. Song and K. Sundmacher, *Engineering*, 2019, **5**, 1017–1026.

7 M. A. El Mrabet, K. El Makkaoui and A. Faize, *2021 4th International Conference on Advanced Communication Technologies and Networking (CommNet)*, 2021, pp. 1–10.

8 I. H. Sarker, *SN Comput. Sci.*, 2021, **2**, 160.

9 R. Vasudevan, G. Pilania and P. V. Balachandran, *J. Appl. Phys.*, 2021, **129**, 070401.

10 Z. Li, J. Yoon, R. Zhang, F. Rajabipour, W. V. S. III, I. Dabo and A. Radlińska, *npj Comput. Mater.*, 2022, **8**, 1–17.

11 J. E. Gubernatis and T. Lookman, *Phys. Rev. Mater.*, 2018, **2**, 120301.

12 J. Schmidt, M. R. G. Marques, S. Botti and M. A. L. Marques, *npj Comput. Mater.*, 2019, **5**, 1–36.

13 T. Zhou, Z. Song and K. Sundmacher, *Engineering*, 2019, **5**, 1017–1026.

14 G. Huang, Y. Guo, Y. Chen and Z. Nie, *Materials*, 2023, **16**, 5977.

15 F. Tanaka, H. Sato, N. Yoshii and H. Matsui, *2018 International Symposium on Semiconductor Manufacturing (ISSM)*, 2018, pp. 1–3.

16 A. Pratap and N. Sardana, *Mater. Today: Proc.*, 2022, **62**, 7341–7347.

17 J. Wei, X. Chu, X. Sun, K. Xu, H.-X. Deng, J. Chen, Z. Wei and M. Lei, *InfoMat*, 2019, **1**, 338–358.

18 S. Hong, C. Liow, J. M. Yuk, H. R. Byon, Y. Yang, E. Cho, J. Yeom, G. Park, H. Kang, S. Kim, Y. S. Shim, M. Na, C. Jeong, G. Hwang, H. Kim, H. Kim, S. Eom, S. Cho, H. Jun, Y. Lee, A. Baucour, K. Bang, M. Kim, S. Yun, J. Ryu, Y. Han, A. Jetybayeva, P. Choi, J. C. Agar, S. V. Kalinin, P. W. Voorhees, P. Littlewood and H.-M. Lee, *ACS Nano*, 2021, **15**, 3971–3995.

19 W. F. Maier, K. Stöwe and S. Sieg, *Angew. Chem.*, 2007, **46**, 6016–6067.

20 A. Ludwig, *npj Comput. Mater.*, 2019, **5**, 1–7.

21 L. Zhao, Y. Zhou, H. Wang, X. Chen, L. Yang, L. Zhang, L. Jiang, Y. H. Jia, X. Chen and H. Wang, *Metall. Mater. Trans. A*, 2021, **52**, 1159–1168.

22 J. Gregoire, L. Zhou and J. A. Haber, *Nat. Synth.*, 2023, **2**, 493–504.

23 K. Shahzad, A. I. Mardare and A. W. Hassel, *Sci. Technol. Adv. Mater.: Methods*, 2024, **4**, 2292486.

24 W. L. Ng, G. L. Goh, G. D. Goh, J. S. J. Ten and W. Y. Yeong, *Adv. Mater.*, 2024, **36**, 2310006.

25 Y. B. Baris Ördek and E. Coatanea, *Prod. Manuf. Res.*, 2024, **12**, 2326526.

26 A. Tran, J. Tranchida, T. Wildey and A. P. Thompson, *J. Chem. Phys.*, 2020, **153 7**, 074705.

27 T. Mueller, A. G. Kusne and R. Ramprasad, *Rev. Comput. Chem.*, 2016, 186–273.

28 B. Sun, M. Fernandez and A. S. Barnard, *Nanoscale Horiz.*, 2016, **1**, 89–95.

29 A. S. Barnard, B. Motevalli, A. J. Parker, J. M. Fischer, C. A. Feigl and G. Opletal, *Nanoscale*, 2019, **11**, 19190–19201.

30 H. Yin, Z. Sun, Z. Wang, D. Tang, C. H. Pang, X. Yu, A. S. Barnard, H. Zhao and Z. Yin, *Cell Rep. Phys. Sci.*, 2021, **2**, 100482.

31 S. Li and A. S. Barnard, *Adv. Theory Simul.*, 2021, **5**, 2100414.

32 A. Challapalli, D. Patel and G. Li, *Mater. Des.*, 2021, **208**, 109937.

33 C. S. Ha, D. Yao, Z. Xu, C. Liu, H. Liu, D. Elkins, M. Kile, V. S. Deshpande, Z. Kong, M. Bauchy and X. R. Zheng, *Nat. Commun.*, 2023, **14**, 5765.

34 J. Lee, D.-O. Park, M. Lee, H. Lee, K. Park, I. Lee and S. W. Ryu, *Mater. Horiz.*, 2023, **10**, 5436–5456.

35 G.-J. Qi and J. Luo, *IEEE Trans. Pattern Anal. Mach. Intell.*, 2019, **44**, 2168–2187.

36 R. Ferrando, J. Jellinek and R. L. Johnston, *Chem. Rev.*, 2008, **108**(3), 845–910.

37 Y. Wang, L. Zhang, B. Xu, X. Wang and H. Wang, *Modell. Simul. Mater. Sci. Eng.*, 2021, **30**, 025003.

38 Z. Yang and W. GAO, *Advanced Science*, 2022, **9**, 2106043.

39 S. Han, G. Barcaro, A. Fortunelli, S. Lysgaard, T. Vegge and H. A. Hansen, *npj Comput. Mater.*, 2022, **8**, 121.

40 Q. Gromoff, P. Benzo, W. A. Saidi, C. M. Andolina, M.-J. Casanove, T. Hungria, S. Barre, M. Benoit and J. Lam, *Nanoscale*, 2024, **16**, 384–393.

41 J. Zhang, X. Liu, S. Bi, J. Yin, G. Zhang and M. Eisenbach, *Mater. Des.*, 2020, **185**, 108247.

42 B. Akhil, A. Bajpai, N. P. Gurao and K. Biswas, *Modell. Simul. Mater. Sci. Eng.*, 2021, **29**, 085005.

43 L. Li, B. Xie, Q. Fang and J. Li, *Metall. Mater. Trans. A*, 2021, **52**, 439–448.

44 A. Pandey, J. G. Gigax and R. Pokharel, *JOM*, 2022, **74**, 2908–2920.

45 G. Hayashi, K. Suzuki, T. Terai, H. Fujii, M. Ogura and K. Sato, *Sci. Technol. Adv. Mater.: Methods*, 2022, **2**, 381–391.

46 X. Liu, J. Zhang and Z. Pei, *Prog. Mater. Sci.*, 2022, **131**, 101018.

47 Z. Rao, P.-Y. Tung, R. Xie, Y. Wei, H. Zhang, A. Ferrari, T. P. C. Klaver, F. Körmann, P. T. Sukumar, A. K. da Silva, Y. Chen, Z. Li, D. Ponge, J. Neugebauer, O. Gutfleisch, S. Bauer and D. Raabe, *Science*, 2022, **378**, 78–85.

48 G. Vazquez, P. K. Singh, D. Sauceda, R. Couperthwaite, N. Britt, K. Youssef, D. D. Johnson and R. Arr'oyave, *Acta Mater.*, 2022, **232**, 117924.

49 Y. Zeng, M. Man, C. K. Ng, D. Wuu, J. J. Lee, F. Wei, P. Wang, K. Bai, D. C. C. Tan and Y.-W. Zhang, *APL Mater.*, 2022, **10**, 101104.

50 S. Kamnis, A. K. Sfikas and S. González, *International Thermal Spray Conference*, 2022, pp. 522–533.

51 U. Bhandari, M. R. Rafi, C. Zhang and S. Yang, *Mater. Today Commun.*, 2020, 101871.

52 J. Wang, H. Kwon, H. S. Kim and B. J. Lee, *npj Comput. Mater.*, 2023, **9**, 1–13.

53 M. Kandavalli, A. Agarwal, A. Poonia, M. Kishor and K. P. R. Ayyagari, *Sci. Rep.*, 2023, **13**, 20504.

54 S. Liu and C. Yang, *Metals*, 2024, **14**, 235.

55 A. B. Mazitov, M. A. Springer, N. Lopanitsyna, G. Fraux, S. De and M. Ceriotti, *J. Phys.: Mater.*, 2023, **7**, 025007.

56 J. Berry, R. M. Snell, M. Anderson, L. R. Owen, O. M. Messé, I. Todd and K. A. Christofidou, *Adv. Eng. Mater.*, 2024, **26**, 2302064.

57 S. Zhao, R. Yuan, W. Liao, Y. Zhao, J. Wang, J. Li and T. Lookman, *J. Mater. Chem. A*, 2024, **12**, 2807–2819.

58 S.-H. V. Oh, S.-H. Yoo and W. Jang, *npj Comput. Mater.*, 2024, **10**, 1–7.

59 P. Rambabu, N. Eswara Prasad, V. Kutumbarao and R. Wanhill, *Aerospace Materials and Material Technologies: Volume 1: Aerospace Materials*, 2017, pp. 29–52.

60 R. Boyer, *Adv. Perform. Mater.*, 1995, **2**, 349–368.

61 M. K. Kulekci, *Int. J. Adv. Des. Manuf. Technol.*, 2008, **39**, 851–865.

62 W. Miller, L. Zhuang, J. Bottema, A. Wittebrood, P. De Smet, A. Haszler and A. Vieregge, *Mater. Sci. Eng. A*, 2000, **280**, 37–49.

63 M. A. Wahid, A. N. Siddiquee and Z. A. Khan, *Mar. Syst. Ocean Technol.*, 2020, **15**, 70–80.

64 R. Willms, *Nordic Steel Construction Conference*, Malmo, Sweden, 2009.

65 S. Magdassi, M. Grouchko and A. Kamyshny, *Materials*, 2010, **3**, 4626–4638.

66 J. S. Faulkner, *Prog. Mater. Sci.*, 1982, **27**, 1–187.

67 F. Habashi, *Alloys: Preparation, Properties, Applications*, John Wiley & Sons, 2008.

68 K.-E. Thelning, *Steel and its Heat Treatment*, Butterworth-Heinemann, 1975, pp. 82–126.

69 J. Westbrook, *Computerization and Networking of Materials Data Bases*, ASTM International, 1989.

70 P. K. Samal, *Powder Metallurgy*, ASM International, 2015, pp. 415–420.

71 I. Polmear, D. StJohn, J.-F. Nie and M. Qian, *Light Alloys: Metallurgy of the Light Metals*, Butterworth-Heinemann, 2017.

72 J. G. Kaufman, in *Understanding Wrought and Cast Aluminum Alloy Designations*, ASM International, 2013, pp. 23–37.

73 J. Christian, *The Theory of Transformations in Metals and Alloys*, Newnes, 2002.

74 H. J. Goldschmid, *Interstitial alloys*, Springer, 2013.

75 D. S. Thompson, *Metall. Trans. A*, 1975, **6**, 671–683.

76 G. S. Upadhyaya, *Powder Metallurgy Technology*, Cambridge Int Science Publishing, 1997.

77 L. Sun, G. Yuan, L. Gao, J. Yang, M. Chhowalla, M. H. Gharahcheshmeh, K. K. Gleason, Y. S. Choi, B. H. Hong and Z. Liu, *Nat. Rev. Methods Primers*, 2021, **1**, 5.

78 J. C.-M. Li, Microstructure and properties of materials, *World Sci.*, 1996, **2**, 1–452.

79 V. B. Ginzburg, *Steel-Rolling Technology: Theory and Practice*, CRC Press, 1989.

80 H. Yoshimura and K. Tanaka, *J. Mater. Process. Technol.*, 2000, **98**, 196–204.

81 D. Edmonds, K. He, F. Rizzo, B. De Cooman, D. Matlock and J. Speer, *Mater. Sci. Eng. A*, 2006, **438**, 25–34.

82 I. Polmear and M. Couper, *Metall. Trans. A*, 1988, **19**, 1027–1035.

83 A. Abu-Odeh, E. Galvan, T. Kirk, H. Mao, Q. Chen, P. Mason, R. Malak and R. Arróyave, *Acta Mater.*, 2018, **152**, 41–57.

84 X. Yang, G. M. El-Fallah, Q. Tao, J. Fu, C. Leng, J. Shepherd and H. Dong, *Mater. Today Commun.*, 2023, **34**, 105162.

85 R. O. Ritchie, *Nat. Mater.*, 2011, **10**, 817–822.

86 J. L. Cann, A. De Luca, D. C. Dunand, D. Dye, D. B. Miracle, H. S. Oh, E. A. Olivetti, T. M. Pollock, W. J. Poole, R. Yang, et al., *Prog. Mater. Sci.*, 2021, **117**, 100722.

87 A. Aversa, G. Marchese, A. Saboori, E. Bassini, D. Manfredi, S. Biamino, D. Ugues, P. Fino and M. Lombardi, *Materials*, 2019, **12**, 1007.

88 Y. Kong, Z. Jia, Z. Liu, M. Liu, H. J. Roven and Q. Liu, *J. Alloys Compd.*, 2021, **857**, 157611.

89 N. Gaudence, N. Aimable, T. Mbuya and B. Mose, *International Journal of Engineering Research & Technology*, 2019, **8**, bIJERTV8IS050281.

90 R. Kaçar and K. Güleryüz, *Mater. Res.*, 2015, **18**, 328–333.

91 A. V. Lozhnikova, P. P. Shchetinin, N. Skrylnikova and N. Redchikova, *Key Eng. Mater.*, 2016, **683**, 15–21.

92 V. Zackay, E. Parker, J. Morris Jr and G. Thomas, *Mater. Sci. Eng.*, 1974, **16**, 201–221.

93 M. J. Donachie and S. Donachie, *Mechanical Engineers Handbook*, 2015, vol. 299.

94 T. M. Pollock and A. Van der Ven, *MRS Bull.*, 2019, **44**, 238–246.

95 G. L. Hart, T. Mueller, C. Toher and S. Curtarolo, *Nat. Rev. Mater.*, 2021, **6**, 730–755.

96 M. Hu, Q. Tan, R. Knibbe, M. Xu, B. Jiang, S. Wang, X. Li and M.-X. Zhang, *Mater. Sci. Eng. R: Rep.*, 2023, **155**, 100746.

97 E. Swann, B. Sun, D. Cleland and A. Barnard, *Mol. Simul.*, 2018, **44**, 905–920.

98 V. Tshitoyan, J. Dagdelen, L. Weston, A. Dunn, Z. Rong, O. Kononova, K. A. Persson, G. Ceder and A. Jain, *Nature*, 2019, **571**, 95–98.

99 C. Sammut and G. I. Webb, in *Clustering*, Springer US, Boston, MA, 2010, p. 180.

100 S. Velliangiri, S. Alagumuthukrishnan and S. I. T. joseph, *Procedia Comput. Sci.*, 2019, **165**, 104–111.

101 B. Motevalli, A. J. Parker, B. Sun and A. S. Barnard, *Nano Futures*, 2019, **3**, 045001.

102 R. Ouyang, S. Curtarolo, E. Ahmetcik, M. Scheffler and L. M. Ghiringhelli, *Phys. Rev. Mater.*, 2018, **2**, 083802.

103 M. A. Bessa, R. Bostanabad, Z. Liu, A. Hu, D. W. Apley, C. Brinson, W. Chen and W. K. Liu, *Comput. Methods Appl. Mech. Eng.*, 2017, **320**, 633–667.

104 M. Wenzlick, O. Mamun, R. Devanathan, K. Rose and J. Hawk, *J. Mater. Eng. Perform.*, 2021, **30**, 823–838.

105 R. Bellman, *Introduction to the mathematical theory of control processes: Linear equations and quadratic criteria*, Elsevier, 2016.

106 X. Huang, L. Wu and Y. Ye, *Int. J. Pattern Recognit. Artif. Intell.*, 2019, **33**, 1950017.

107 R. Jha, G. S. Dulikravich, N. Chakraborti, M. Fan, J. Schwartz, C. C. Koch, M. J. Colaco, C. Poloni and I. N. Egorov, *Mater. Manuf. Processes*, 2017, **32**, 1067–1074.

108 I. Toda-Caraballo, E. I. Galindo-Nava and P. E. Rivera-Díaz-del Castillo, *J. Alloys Compd.*, 2013, **566**, 217–228.

109 J. P. Stevens, *Psychol. Bull.*, 1984, **95**, 334.

110 E. Acuña and C. Rodriguez, in *A Meta analysis study of outlier detection methods in classification*, University of Puerto Rico at Mayaguez, 2004, vol. 15.

111 T. Liu, Z. Y. Tho and A. S. Barnard, *Digital Discovery*, 2024, **3**, 422–435.

112 L. Tian, Y. Fan, L. Li and N. Mousseau, *Scr. Mater.*, 2020, **186**, 185–189.

113 M. Wenzlick, O. Mamun, R. Devanathan, K. Rose and J. Hawk, *Jom*, 2022, **74**, 2846–2859.

114 G. L. W. Hart, T. Mueller, C. Toher and S. Curtarolo, *Nat. Rev. Mater.*, 2021, **6**, 730–755.

115 J. F. Durodola, *Prog. Mater. Sci.*, 2021, 100797.

116 X. Liu, P. Xu, J. Zhao, W. Lu, M. Li and G. Wang, *J. Alloys Compd.*, 2022, **921**, 165984.

117 H. Fu, H. Zhang, C. Wang, W. Yong and J.-X. Xie, *Int. J. Miner., Metall. Mater.*, 2022, **29**, 635–644.

118 M. Hu, Q. Tan, R. Knibbe, M. Xu, B. Jiang, S. Wang, X. Li and M. Zhang, *Mater. Sci. Eng. R: Rep.*, 2023, **155**, 100746.

119 B. Sun, M. Fernández and A. S. Barnard, *J. Chem. Inf. Model.*, 2017, **57**(10), 2413–2423.

120 A. S. Mangsor, Z. H. Rizvi, K. T. Chaudhary and M. S. Aziz, *J. Phys.: Conf. Ser.*, 2018, **1027**, 012017.

121 B. Sun and A. S. Barnard, *J. Phys.: Mater.*, 2018, **1**, 016001.

122 A. A. Shirinyan, V. K. Kozin, J. Hellsvik, M. Pereiro, O. Eriksson and D. Yudin, *Phys. Rev. B*, 2019, **99**, 041108.

123 A. K. Verma, W.-H. Huang, J. A. Hawk, L. S. Bruckman, R. H. French, V. Romanov and J. L. Carter, *Mater. Sci. Eng. A*, 2019, **763**, 138142.

124 R. Jha and G. S. Dulikravich, *Metals*, 2019, **9**, 537.

125 N. Krishnamurthy, S. Maddali, J. A. Hawk and V. N. Romanov, *Comput. Mater. Sci.*, 2019, **168**, 268–279.

126 A. K. Verma, J. A. Hawk, L. S. Bruckman, R. H. French, V. Romanov and J. L. Carter, *Metall. Mater. Trans. A*, 2019, **50**, 3106–3120.

127 B. Sun and A. S. Barnard, *J. Phys.: Mater.*, 2019, **2**, 034003.

128 A. J. Parker, G. Opletal and A. S. Barnard, *J. Appl. Phys.*, 2020, **128**, 014301.

129 A. Dasgupta, Y. Gao, S. R. Broderick, E. B. Pitman and K. Rajan, *J. Phys. Chem. C*, 2020, **124**, 14158–14166.

130 L. Tian, Y. Fan, L. Li and N. Mousseau, *Scr. Mater.*, 2020, **186**, 185–189.

131 A. J. Parker, B. Motevalli, G. Opletal and A. S. Barnard, *Nanotechnology*, 2020, **32**, 095404.

132 J. A. Esterhuizen, B. R. Goldsmith and S. Linic, *Chem Catal.*, 2021, **1**, 923–940.

133 J. Jung, J. I. Yoon, H. K. Park, H. Jo and H. S. Kim, *Materialia*, 2020, **11**, 100690.

134 C. Liu, E. Fujita, Y. Katsura, Y. Inada, A. Ishikawa, R. Tamura, K. Kimura and R. Yoshida, *Adv. Mater.*, 2021, **33**, 2102507.

135 J. A. Esterhuizen, B. R. Goldsmith and S. Linic, *Chem Catal.*, 2021, **1**, 923–940.

136 R. Subbarao, *et al.*, *Mater. Today: Proc.*, 2021, **46**, 8615–8620.

137 Y. Kim, H. K. Park, J. Jung, P. Asghari-Rad, S. Lee, J. Y. Kim, H. G. Jung and H. S. Kim, *Mater. Des.*, 2021, **202**, 109544.

138 J. Yin, Z. Pei and M. C. Gao, *Nat. Comput. Sci.*, 2021, **1**, 686–693.

139 K. Lee, M. V. Ayyasamy, P. Delsa, T. Q. Hartnett and P. V. Balachandran, *npj Comput. Mater.*, 2022, **8**, 25.

140 S. Chintakindi, A. Alsamhan, M. H. Abidi and M. P. Kumar, *Int. J. Comput. Intell. Syst.*, 2022, **15**, 18.

141 K. Lee, M. V. Ayyasamy, Y. Ji and P. V. Balachandran, *Sci. Rep.*, 2022, **12**, 11591.

142 Z. C. Xin, J. S. Zhang, Y. Jin, J. Zheng and Q. Liu, *Int. J. Miner., Metall. Mater.*, 2022, **30**, 335–344.

143 A. S. Bundela and M. Rahul, *Metall. Mater. Trans. A*, 2022, **53**, 3512–3519.

144 A. L. Foggiatto, Y. Mizutori, T. Yamazaki, S. Sato, K. Masuzawa, R. Nagaoka, M. Taniwaki, S. Fujieda, S. Suzuki, K. Ishiyama, *et al.*, *IEEE Trans. Magn.*, 2023, **59**, 2501604.

145 O. Ahmad, N. Kumar, R. Mukherjee and S. Bhowmick, *Phys. Rev. Mater.*, 2023, **7**, 083802.

146 N. Bhat, A. S. Barnard and N. Birbilis, *R. Soc. Open Sci.*, 2023, **10**, 220360.

147 M. Ghorbani, M. Boley, P. Nakashima and N. Birbilis, *J. Magnesium Alloys*, 2023, **11**, 3620–3633.

148 H.-F. Chen, Y.-P. Yang, W.-L. Chen, P. J. Wang, W. Lai, Y.-K. Fuh and T. T. Li, *Mater. Chem. Phys.*, 2023, **295**, 127070.

149 T. Tiwari, S. Jalalian, C. L. Mendis and D. G. Eskin, *JOM*, 2023, **75**, 4526–4537.

150 J. Y. C. Ting, A. J. Parker and A. S. Barnard, *Chem. Mater.*, 2023, **35**, 728–738.

151 C. Roncaglia and R. Ferrando, *J. Chem. Inf. Model.*, 2023, **63**, 459–473.

152 B. Vela, C. Acemi, P. Singh, T. Kirk, W. Trehern, E. Norris, D. D. Johnson, I. Karaman and R. Arróyave, *Acta Mater.*, 2023, **248**, 118784.

153 S. Fetni, T. Q. D. Pham, T. V. Hoang, H. S. Tran, L. Duchêne, X.-V. Tran and A. M. Habraken, *Comput. Mater. Sci.*, 2023, **216**, 111820.

154 A. Moses, X. Peng, S. Wang and D. Chen, *JOM*, 2024, **76**, 4388–4403.

155 X. Liu, Y. Bao, L. Zhao and C. Gu, *J. Sustain. Metall.*, 2024, **10**, 509–524.

156 A. Usuga, C. Praveen and A. Comas-Vives, *J. Mater. Chem. A*, 2024, **12**, 2708–2721.

157 B. Venkatesh and J. Anuradha, *Cybern. Inf. Technol.*, 2019, **19**, 3–26.

158 C. Yang, C. Ren, Y. Jia, G. Wang, M. Li and W. Lu, *Acta Mater.*, 2022, **222**, 117431.

159 J. Li, K. Cheng, S. Wang, F. Morstatter, R. P. Trevino, J. Tang and H. Liu, *ACM Computing Surveys (CSUR)*, 2017, 50, 1–45.

160 K. Kira and L. A. Rendell, *Machine Learning Proceedings 1992*, Elsevier, 1992, pp. 249–256.

161 J. G. Dy and C. E. Brodley, *J. Mach. Learn. Res.*, 2004, **5**, 845–889.

162 N. Bhat, A. S. Barnard and N. Birbilis, *J. Mater. Sci.*, 2024, **59**, 1448–1463.

163 A. Altmann, L. Toloşi, O. Sander and T. Lengauer, *Bioinformatics*, 2010, **26**, 1340–1347.

164 K. V. Priyadharshini, A. Vijay, K. Swaminathan, T. Avudaiappan and V. Banupriya, *Mater. Today: Proc.*, 2022, **69**, 710–715.

165 P.-P. D. Breuck, G. Hautier and G. Rignanese, *npj Comput. Mater.*, 2020, **7**, 1–8.

166 B. Hoock, S. Rigamonti and C. Draxl, *New J. Phys.*, 2022, **24**, 113049.

167 H. Abdi and L. J. Williams, *Wiley Interdiscip. Rev. Comput. Stat.*, 2010, **2**, 433–459.

168 S. Schneider, S. G. Schneider, H. M. d. Silva and C. d. Moura Neto, *Mater. Res.*, 2005, **8**, 435–438.

169 H. Xu, C. Caramanis and S. Mannor, *IEEE Trans. Inf. Theory*, 2012, **59**, 546–572.

170 K. Rajan, C. Suh and P. F. Mendez, *Stat. Anal. Data Min.*, 2009, **1**, 361–371.

171 V. Klema and A. J. Laub, *IEEE Trans. Autom. Control*, 1980, **25**, 164–176.

172 B. P. Epps and E. M. Krivitzky, *Exp. Fluids*, 2019, **60**, 1–23.

173 M. Brand, *Computer Vision—ECCV 2002: 7th European Conference on Computer Vision*, Copenhagen, Denmark, 2002, pp. 707–720.

174 H. Swathi, S. Sohini, Surbhi and G. Gopichand, *IOP Conf. Ser.: Mater. Sci. Eng.*, 2017, **263**, 042082.

175 C. Zhang, R. Han, A. Zhang and P. Voyles, *Microsc. Microanal.*, 2020, **26**, 1722–1723.

176 A. Cutler and L. Breiman, *Technometrics*, 1994, **36**, 338–347.

177 S. Mair and U. Brefeld, *33rd Conference on Neural Information Processing Systems*, Vancouver, Canada, 2019.

178 M. Fernandez and A. S. Barnard, *ACS Nano*, 2015, **9**, 11980–11992.

179 M. Fernandez, H. F. Wilson and A. S. Barnard, *Nanoscale*, 2017, **9**, 832–843.

180 T. Kohonen, *Proc. IEEE*, 1990, **78**, 1464–1480.

181 C. Bishop, *Clarendon Press google scholar*, 1995, 2, pp. 223–228.

182 A. S. Barnard, B. Motevalli and B. Sun, *MRS Commun.*, 2019, **9**, 730–736.

183 B. Sun and A. S. Barnard, *J. Phys.: Mater.*, 2018, **1**, 016001.

184 P. Wittek, S. C. Gao, I. S. Lim and L. Zhao, *arXiv*, preprint, arXiv:1305.1422, 2013, DOI: **10.18637/jss.v078.i09**.

185 W. Gardner, R. Maliki, S. M. Cutts, B. W. Muir, D. Ballabio, D. A. Winkler and P. J. Pigram, *Anal. Chem.*, 2020, **92**, 10450–10459.

186 S. Y. Wong, S. L. Harmer, W. Gardner, A. K. Schenk, D. Ballabio and P. J. Pigram, *Adv. Mater. Interfaces*, 2023, **10**, 10450–10459.

187 S. E. Bamford, W. Gardner, D. A. Winkler, B. W. Muir, D. Alahakoon and P. J. Pigram, *J. Am. Soc. Mass Spectrom.*, 2024, **35**, 2516–2528.

188 D. Bank, N. Koenigstein and R. Giryes, *Machine Learning for Data Science Handbook: Data Mining and Knowledge Discovery Handbook*, 2023, pp. 353–374.

189 W. Wang, Y. Huang, Y. Wang and L. Wang, *Proceedings of the IEEE Conference on Computer Vision and Pattern Recognition Workshops*, 2014, pp. 490–497.

190 M. Sakurada and T. Yairi, *Proceedings of the MLSDA 2014 2nd Workshop on Machine Learning for Sensory Data Analysis*, 2014, pp. 4–11.

191 Q. Meng, D. Catchpoole, D. Skillicom and P. J. Kennedy, *2017 International Joint Conference on Neural Networks (IJCNN)*, 2017, pp. 364–371.

192 Y. Wang, H. Yao and S. Zhao, *Neurocomputing*, 2016, **184**, 232–242.

193 E. Ordway-West, P. Parveen and A. Henslee, *2018 IEEE International Congress on Big Data (BigData Congress)*, 2018, pp. 205–209.

194 J. Baima, A. M. Goryaeva, T. D. Swinburne, J.-B. Maillet, M. Nastar and M.-C. Marinica, *Phys. Chem. Chem. Phys.*, 2022, **24**, 23152–23163.

195 S. Fetni, T. Q. D. Pham, T. V. Hoang, H. S. Tran, L. Duchêne, X.-V. Tran and A. M. Habraken, *Comput. Mater. Sci.*, 2023, **216**, 111820.

196 A. Choudhury, Y. C. Yabansu, S. R. Kalidindi and A. Dennstedt, *Acta Mater.*, 2016, **110**, 131–141.

197 A. S. Mangsor, Z. H. Rizvi, K. Chaudhary and M. S. Aziz, *J. Phys.: Conf. Ser.*, 2018, 012017.

198 Z. Zhuang and A. S. Barnard, *Chem. Mater.*, 2023, **35**, 9325–9338.

199 B. Motevalli, A. J. Parker, B. Sun and A. S. Barnard, *Nano Futures*, 2019, **3**, 045001.

200 Y. Ji, A. Koeppe, P. Altschuh, D. Rajagopal, Y. Zhao, W. Chen, Y. Zhang, Y. Zheng and B. Nestler, *Comput. Mater. Sci.*, 2024, **232**, 112628.

201 X. Huo and A. Smith, Series on Computers and Operations Research, in, *Recent Advances in Data Mining of Enterprise Data: Algorithms and Applications*, 2008, pp. 691–745.

202 J. B. Kruskal, *Psychometrika*, 1964, **29**, 115–129.

203 S. T. Roweis and L. K. Saul, *Science*, 2000, **290**(5500), 2323–2326.

204 J. B. Tenenbaum, V. de Silva and J. C. Langford, *Science*, 2000, **290**(5500), 2319–2323.

205 M. Belkin and P. Niyogi, *Neural Comput.*, 2003, **15**, 1373–1396.

206 L. McInnes, J. Healy, N. Saul and L. Großberger, *J. Open Source Softw.*, 2018, **3**, 861.

207 L. van der Maaten, *J. Mach. Learn. Res.*, 2014, **15**, 3221–3245.

208 A. S. Barnard and G. Opletal, *Nanoscale*, 2019, **11**, 23165–23172.

209 D. Kobak and G. C. Linderman, *Nat. Biotechnol.*, 2021, **39**, 156–157.

210 L. Van der Maaten and G. Hinton, *J. Mach. Learn. Res.*, 2008, **9**, 2579–2605.

211 L. McInnes, J. Healy, N. Saul and L. Großberger, *J. Open Source Softw.*, 2018, **3**, 861.

212 E. Becht, L. McInnes, J. Healy, C.-A. Dutertre, I. W. Kwok, L. G. Ng, F. Ginhoux and E. W. Newell, *Nat. Biotechnol.*, 2019, **37**, 38–44.

213 S. Kim, L. Zhang, S.-H. Kim and Y. S. Choi, *Met. Mater. Int.*, 2024, **30**, 1817–1830.

214 T. Zhang, R. Ramakrishnan and M. Livny, *ACM SIGMOD Conference*, 1996, pp. 103–114.

215 M. Wenzlick, O. Mamun, R. Devanathan, K. K. Rose and J. A. Hawk, *J. Mater. Eng. Perform.*, 2021, 1–16.

216 X. Liu, X. Qu, X. Xie, S. Li, Y. Bao and L. Zhao, *Processes*, 2024, **12**, 974.

217 K. Li, B. DeCost, K. Choudhary, M. Greenwood and J. Hattrick-Simpers, *npj Comput. Mater.*, 2023, **9**, 55.

218 A. J. Parker and A. S. Barnard, *Nanoscale Horiz.*, 2020, **5**, 1394–1399.

219 A. J. Parker and A. S. Barnard, *Nanoscale Horiz.*, 2021, **6**, 277–282.

220 P. Karande, B. Gallagher and T. Y.-J. Han, *Chem. Mater.*, 2022, **34**, 7650–7665.

221 S. S. Chong, Y. S. Ng, H. Wang and J.-C. Zheng, *Front. Phys.*, 2023, **19**, 13501.

222 R. Xu and D. Wunsch, *IEEE Trans. Neural Netw.*, 2005, **16**, 645–678.

223 A. E. Ezugwu, A. M. Ikotun, O. O. Oyelade, L. Abualigah, J. O. Agushaka, C. I. Eke and A. A. Akinyelu, *Eng. Appl. Artif. Intell.*, 2022, **110**, 104743.

224 D. Xu and Y. jie Tian, *Ann. Data Sci.*, 2015, **2**, 165–193.

225 V. V. Romanuke, *Decis. Mak.: Appl. Manag. Eng.*, 2023, **6**, 734–746.

226 C. Liu, *J. Multivar. Anal.*, 1999, **69**, 206–217.

227 M. Ester, H.-P. Kriegel, J. Sander and X. Xu, *Knowledge Discovery and Data Mining*, 1996, pp. 226–231.

228 F. Murtagh and P. Contreras, *Wiley Interdiscip. Rev.: Data Min. Knowl. Discov.*, 2012, **2**, 86–97.

229 E. Hartuv and R. Shamir, *Inf. Process. Lett.*, 2000, **76**, 175–181.

230 T. Xiang and S. Gong, *Pattern Recognit.*, 2008, **41**, 1012–1029.

231 M.-S. Yang, *Math. Comput. Model.*, 1993, **18**, 1–16.

232 S. K. Uppada, *International Journal of Computer Science and Information Technologies*, 2014, **5**, 7309–7313.

233 J. MacQueen *et al.*, *Proceedings of the fifth Berkeley symposium on mathematical statistics and probability*, 1967, pp. 281–297.

234 D. Xu and Y. Tian, *Ann. Data Sci.*, 2015, **2**, 165–193.

235 D. A. Reynolds *et al.*, *Encyclopedia of biometrics*, 2009, 741.

236 G. Xuan, W. Zhang and P. Chai, *Proceedings 2001 International Conference on Image Processing (Cat. No. 01CH37205)*, 2001, pp. 145–148.

237 M. Ester, H.-P. Kriegel, J. Sander, X. Xu *et al.*, *Proceedings of Knowledge Discovery and Data Mining*, 1996, pp. 226–231.

238 M. Roux, *J. Classif.*, 2018, **35**, 345–366.

239 A. Guénoche, P. Hansen and B. Jaumard, *J. Classif.*, 1991, **8**, 5–30.

240 A. Bouguettaya, Q. Yu, X. Liu, X. Zhou and A. Song, *Expert Syst. Appl.*, 2015, **42**, 2785–2797.

241 J. H. Ward Jr, *J. Am. Stat. Assoc.*, 1963, **58**, 236–244.

242 F. Murtagh and P. Legendre, *J. Classif.*, 2014, **31**, 274–295.

243 G. M. Downs and J. M. Barnard, *Rev. Comput. Chem.*, 2002, **18**, 1–40.

244 A. Ng, M. Jordan and Y. Weiss, *NIPS'01: Proceedings of the 14th International Conference on Neural Information Processing Systems: Natural and Synthetic*, 2001, vol. 14, pp. 849–856.

245 S. Pettie, in *Minimum Spanning Trees*, ed. M.-Y. Kao, Springer US, Boston, MA, 2008, pp. 541–544.

246 O. Borůvka, *Práce Mor. Přírodověd. Spol.*, 1926, **3**, 37–58.

247 R. L. Thorndike, *Psychometrika*, 1953, **18**, 267–276.

248 P. J. Rousseeuw, *J. Comput. Appl. Math.*, 1987, **20**, 53–65.

249 D. L. Davies and D. W. Bouldin, *IEEE Trans. Pattern Anal. Mach. Intell.*, 1979, 224–227.

250 T. Caliński and J. Harabasz, *Communications in Statistics-theory and Methods*, 1974, **3**, 1–27.

251 F. Orlando Morais, K. F. Andriani and J. L. Da Silva, *J. Chem. Inf. Model.*, 2021, **61**, 3411–3420.

252 T. Tiwari, S. Jalalian, C. Mendis and D. Eskin, *JOM*, 2023, **75**, 4526–4537.

253 M. T. Ribeiro, S. Singh and C. Guestrin, *Proceedings of the 22nd ACM SIGKDD International Conference on Knowledge Discovery and Data Mining*, San Francisco, CA, USA, 2016, pp. 1135–1144.

254 A. de Moura and A. Esteves, *SPAL*, 2013, **2**, 1.

255 G. S. Thoppil, J.-F. Nie and A. Alankar, *Comput. Mater. Sci.*, 2023, **216**, 111855.

256 Z. Li, G. P. Wellawatte, M. Chakraborty, H. A. Gandhi, C. Xu and A. D. White, *Chem. Sci.*, 2020, **11**, 9524–9531.

257 A. Glielmo, B. E. Husic, A. Rodriguez, C. Clementi, F. Noé and A. Laio, *Chem. Rev.*, 2021, **121**, 9722–9758.

258 J. L. Phillips, M. E. Colvin and S. Newsam, *BMC Bioinf.*, 2011, **12**, 1–23.

259 N. M. R. Suri, M. N. Murty and G. Athithan, *Outlier detection: techniques and applications*, Springer, 2019.

260 M. A. Pimentel, D. A. Clifton, L. Clifton and L. Tarassenko, *Signal Process.*, 2014, **99**, 215–249.

261 V. Chandola, A. Banerjee and V. Kumar, *ACM Computing Surveys (CSUR)*, 2009, vol. 41, pp. 1–58.

262 A. M. Jabbar and I. J. Electr, *Electron. Eng.*, 2021, **17**, 76–87.

263 X. Song, M. Wu, C. Jermaine and S. Ranka, *IEEE Trans. Knowl. Data Eng.*, 2007, **19**, 631–645.

264 A. S. Hadi and A. Imon, *J. Stat. Sci.*, 2018, **16**, 87–96.

265 J. Tukey, *Exploratory Data Analysis*, 1977.

266 P. H. Thah and I. S. Sitanggang, *Procedia Environ. Sci.*, 2016, **33**, 258–268.

267 K.-H. Lai, D. Zha, J. Xu, Y. Zhao, G. Wang and X. Hu, *Thirty-Fifth Conference On Neural Information Processing Systems Datasets and Benchmarks Track (Round 1)*, 2021.

268 M. A. Fischler and R. C. Bolles, *Commun. ACM*, 1981, **24**, 381–395.

269 S. Saxena and D. S. Rajpoot, *Advances in Signal Processing and Communication: Select Proceedings of ICSC 2018*, 2019, pp. 281–291.

270 C. Noble and D. Cook, *Proceedings of the 9th ACM SIGKDD International Conference on Knowledge Discovery and Data Mining*. ACM Press, 2003, pp. 631–636.

271 S. J. Shin, J. hong Lee, S. Jadhav and D. B. Kim, *Int. J. Precis. Eng. Manuf.-Smart Tech.*, 2023, 1–26.

272 D. Gunasegaram, A. Barnard, M. Matthews, B. Jared, A. Andreaco, K. Bartsch and A. Murphy, *Addit. Manuf.*, 2024, **81**, 104013.

273 N. Samadiani, A. S. Barnard, D. R. Gunasegaram and N. Fayyazifar, *J. Intell. Manuf.*, 2024, DOI: **10.1007/s10845-024-02490-4**.

274 J. E. Van Engelen and H. H. Hoos, *Mach. Learn.*, 2020, **109**, 373–440.

275 Y.-F. Li and D.-M. Liang, *Front. Comput. Sci.*, 2019, **13**, 669–676.

276 H. Huo, Z. Rong, O. Kononova, W. Sun, T. Botari, T. He, V. Tshitoyan and G. Ceder, *npj Comput. Mater.*, 2019, **5**, 62.

277 F. A. Laskowski, D. B. McHaffie and K. A. See, *Energy Environ. Sci.*, 2023, **16**, 1264–1276.

278 A. Barnard and A. Parker, *CSIRO Software Collection*, 2019.

279 A. J. Parker and A. S. Barnard, *Adv. Theory Simul.*, 2019, **2**, 1900145.

280 A. J. Parker and A. S. Barnard, *Nanoscale Horiz.*, 2020, **5**, 1394–1399.

281 A. Dobra, in *Decision Tree Classification*, ed. L. LIU and M. T. ÖZSU, Springer US, Boston, MA, 2009, pp. 765–769.

282 N. Bhat, A. S. Barnard and N. Birbilis, *Comput. Mater. Sci.*, 2023, **228**, 112270.

283 N. Bhat, A. S. Barnard and N. Birbilis, *Metals*, 2024, **14**, 239.

284 W. Yan, S. Lin, O. L. Kafka, Y. Lian, C. Yu, Z. Liu, J. Yan, S. Wolff, H. Wu, E. Ndip-Agbor, *et al.*, *Comput. Mech.*, 2018, **61**, 521–541.

285 J.-C. Stinville, J. Hestroffer, M.-A. Charpagne, A. Polonsky, M. Echlin, C. Torbet, V. Valle, K. Nygren, M. Miller, O. Klaas, *et al.*, *Scientific Data*, 2022, **9**, 460.

286 A. Glielmo, B. E. Husic, A. Rodriguez, C. Clementi, F. Noé and A. Laio, *Chem. Rev.*, 2021, **121**, 9722–9758.

287 Y.-C. Chang, X. Wang, J. Wang, Y. Wu, K. Zhu, H. Chen, L. Yang, X. Yi, C. Wang, Y. Wang, W. Ye, Y. Zhang, Y. Chang, P. S. Yu, Q. Yang and X. Xie, *ACM Trans. Intell. Syst. Technol.*, 2023, **15**, 1–45.

288 G. A. Pinheiro, J. L. F. D. Silva, M. D. Soares and M. G. Quiles, *Computational Science and Its Applications – ICCSA 2020*, 2020, 12249, pp. 421 – 433.

289 C. T. Cai, A. J. Parker and A. S. Barnard, *J. Phys.: Mater.*, 2024, **7**, 022005.

290 T. Houben, T. Huisman, M. Pisarenco, F. van der Sommen and P. H. N. de With, *J. Micro/Nanopatterning, Mater., Metrol.*, 2023, **22**, 031208.

291 Z. Yang, X. Li, L. C. Brinson, A. N. Choudhary, W. Chen and A. Agrawal, *J. Mech. Des.*, 2018, **140**, 111416.

292 J. M. Fischer, A. J. Parker and A. S. Barnard, *J. Phys.: Mater.*, 2021, **4**, 041001.

293 R. Magar, Y. Wang and A. B. Farimani, *npj Comput. Mater.*, 2022, **8**, 1–8.

294 A. New, N. Q. Le, M. J. Pekala and C. D. Stiles, *arXiv*, preprint, arXiv: abs/2408.17255, 2024, DOI: **10.48550/arXiv.2408.17255**.

295 T. Koker, K. Quigley, W. Spaeth, N. C. Frey and L. Li, *Graph Contrastive Learning for Materials*, 2022.

296 G. S. Na and H. W. Kim, *Chem. commun.*, 2022, **58**, 6729–6732.

297 C. Chen, S. J. L. Wong, E. T. Zhi'En and H. Li, *Mater. Des.*, 2024, **244**, 113115.